

Global Fits of the SM and MSSM to Electroweak Precision Data

W. de Boerⁱ¹, A. Dabelsteinⁱⁱⁱ², W. Hollikⁱⁱ³,
W. Mösleⁱⁱ⁴, U. Schwickerathⁱ⁵,

*i) Inst. für Experimentelle Kernphysik, Univ. Karlsruhe,
Postfach 6980, D-76128 Karlsruhe, Germany*

*ii) Inst. für Theoretische Physik, Univ. Karlsruhe,
Postfach 6980, D-76128 Karlsruhe, Germany*

*iii) Inst. für Theoretische Physik, Univ. München,
James Franck Straße, D-85747 Garching, Germany*

Abstract

A program including all radiative corrections to the Minimal Supersymmetric Standard Model (MSSM) at the same level as the radiative corrections to the Standard Model (SM) has been developed and used to perform global fits to all electroweak data from LEP, SLC and the Tevatron and the radiative $b \rightarrow s\gamma$ decay from CLEO. Values of the strong coupling constant at the M_Z scale and $\sin^2 \theta_{\overline{MS}}$ are derived, both in the SM and MSSM.

Recent updates on electroweak data, which have been presented at the Warsaw Conference in summer 1996, reduce the too high branching ratio of the Z^0 boson into b-quarks in the SM from a 3.2σ to a 1.8σ effect. In addition, the $b \rightarrow s\gamma$ decay is 30% below the SM prediction. In the MSSM light stops and light charginos increase R_b and decrease the $b \rightarrow s\gamma$ rate, so both observations can be brought into agreement with the MSSM for the same region of parameter space. However, the resulting χ^2 value for the MSSM fits is only marginally lower and in addition, the splitting in the stop sector has to be unnaturally high.

¹Email: wim.de.boer@cern.ch

²E-mail: Andreas.Dabelstein@tu-muenchen.de

³E-mail: hollik@itpaxp3.physik.uni-karlsruhe.de

⁴E-mail: wm@itpaxp1.physik.uni-karlsruhe.de

⁵E-mail: Ulrich.Schwickerath@cern.ch

1 Introduction

Supersymmetry presupposes a symmetry between fermions and bosons, which can be implemented in the Standard Model (SM) by introducing a fermion for each boson and vice versa[1]. In this case the problem of quadratic divergent radiative corrections to the Higgs boson masses is solved, since fermions and bosons contribute with an opposite sign to the loop corrections. These new supersymmetric particles (“sparticles”) contribute additionally to the radiative corrections and can influence electroweak precision variables, like e.g. $R_b = \Gamma_{Z^0 \rightarrow b\bar{b}}/\Gamma_{Z^0 \rightarrow \text{hadrons}}$ or the penguin mediated decay $b \rightarrow s\gamma$. Radiative corrections have been calculated in the Minimal Supersymmetric Standard Model (MSSM) to nearly the same level as in the SM, so an equivalent analysis of all electroweak data can be performed both in the SM and MSSM. In this paper such analysis are described using data from Tevatron [2, 3], LEP and SLC [4, 5], the measurement of $R_{b \rightarrow s\gamma} = \frac{BR(b \rightarrow s\gamma)}{BR(b \rightarrow ce\bar{\nu})}$ from CLEO [6] and limits on the masses of supersymmetric particles [7, 8, 9, 10, 11]. For the SM predictions the ZFITTER program[12] was used, while for the MSSM predictions the SUSYFITTER program[13], which will be discussed below, was used. In both cases MINUIT[14] was used as χ^2 minimizer in order to obtain the optimum parameter values. For all SUSY masses well above the electroweak scale one does not expect significant differences between the SM and the MSSM predictions.

Previous LEP data [5] showed a too high value of R_b (3.2σ) and a too low value of R_c (2σ). It has been shown by several groups[15]-[23] that it is possible to increase R_b in the MSSM with light charginos, top squarks or Higgses, which yield large positive contributions to the $Zb\bar{b}$ vertex because of the large Yukawa couplings of the third generation. The first two generations are not affected by such corrections, so no modifications in R_c can be obtained. Recent updates of electroweak data, presented at the Warsaw Conference[4], show no deviation of R_c anymore and a value of R_b which is 1.8σ above the SM value. In addition, the experimental value for $R_{b \rightarrow s\gamma} = \frac{BR(b \rightarrow s\gamma)}{BR(b \rightarrow ce\bar{\nu})}$ from CLEO [6] equals $(2.32 \pm 0.67) \cdot 10^{-4}$, which is about 30% below the SM prediction after taking the ca. 10% increase in the prediction by the next-to-leading-log contributions into account[24].

In the MSSM an increase in R_b can cause a decrease in the $b \rightarrow s\gamma$ rate, since both cases involve similar diagrams usually with an opposite sign, e.g. the $\tilde{t} - \tilde{t} - \chi^\pm$ vertex corrections in $Z^0 \rightarrow b\bar{b}$ and the $\tilde{t} - \chi^\pm$ loop corrections in $b \rightarrow s\gamma$ have an opposite sign. Both, the too high value of R_b and the too low value of $b \rightarrow s\gamma$ prefer a chargino mass around 90 GeV and a stop mass around 50 GeV or alternatively light Higgses around 50 GeV, so both observations agree with the MSSM for the same region of parameter space, albeit an unnatural one, as will be shown.

2 Radiative Corrections in the MSSM

At the Z boson resonance two classes of precision observables are available:

a) inclusive quantities:

- the partial leptonic and hadronic decay width $\Gamma_{f\bar{f}}$,
- the total decay width Γ_Z ,

- the hadronic peak cross section σ_h ,
- the ratio of the hadronic to the electronic decay width of the Z boson: R_h ,
- the ratio of the partial decay width for $Z \rightarrow c\bar{c}(b\bar{b})$ to the hadronic width, R_c , R_b .

b) asymmetries and the corresponding mixing angles:

- the *forward-backward* asymmetries A_{FB}^f ,
- the *left-right* asymmetries A_{LR}^f ,
- the τ polarization P_τ ,

This set of precision observables together with the $R_{b \rightarrow s\gamma}$ rate[6], the W - and the top mass is convenient for a numerical analysis of the supersymmetric parameter space. In the following the observables defined above are expressed with the help of effective couplings.

2.1 The effective Z - f - f couplings

The coupling of the Z boson to fermions f can be expressed by effective vector and axial vector coupling constants v_{eff}^f, a_{eff}^f in terms of the NC vertex:

$$J_{NC}^\mu = \frac{e}{2s_W c_W} \gamma^\mu (v_{eff}^f - a_{eff}^f \gamma_5) , \quad (1)$$

where the convention is introduced : $c_W^2 = \cos^2 \theta_W = 1 - s_W^2 = M_W^2/M_Z^2$ [25]. Input parameters are the μ decay constant $G_\mu = 1.166392 \times 10^{-5} \text{ GeV}^{-2}$, $\alpha_{EM} = 1/137.036$ and the mass of the Z^0 boson $M_Z = 91.1884 \text{ GeV}$. The mass of the W boson is related to these input parameters through:

$$\frac{G_\mu}{\sqrt{2}} = \frac{\pi \alpha_{EM}}{2s_W^2 M_W^2} \cdot \frac{1}{1 - \Delta r_{MSSM}(\alpha_{EM}, M_W, M_Z, m_t, \dots)} , \quad (2)$$

where the complete MSSM one-loop contributions are parameterized by the quantity Δr_{MSSM} [26]. Leading higher order SM corrections[27, 28] to the quantity Δr are included in the calculation.

The effective couplings v_{eff}^f, a_{eff}^f can be written as:

$$\begin{aligned} v_{eff}^f &= \sqrt{Z_Z} (v^f + \Delta v^f + Z_M Q_f) \\ a_{eff}^f &= \sqrt{Z_Z} (a^f + \Delta a^f) . \end{aligned} \quad (3)$$

v^f and a^f are the tree-level vector and axial vector couplings:

$$v^f = I_3^f - 2Q_f s_W^2 , \quad a^f = I_3^f . \quad (4)$$

Z_Z, Z_M are given in eq. (10). The complete MSSM one-loop contributions of the non-universal finite vector and axial vector couplings $\Delta v^f, \Delta a^f$ have been calculated[13], together with the leading two-loop Standard Model contributions[27, 28, 29]. They are derived in the

't Hooft-Feynman gauge and in the on-shell renormalization scheme[30]. Fig. 1 shows the MSSM one-loop $Z \rightarrow f\bar{f}$ vertex correction diagrams.

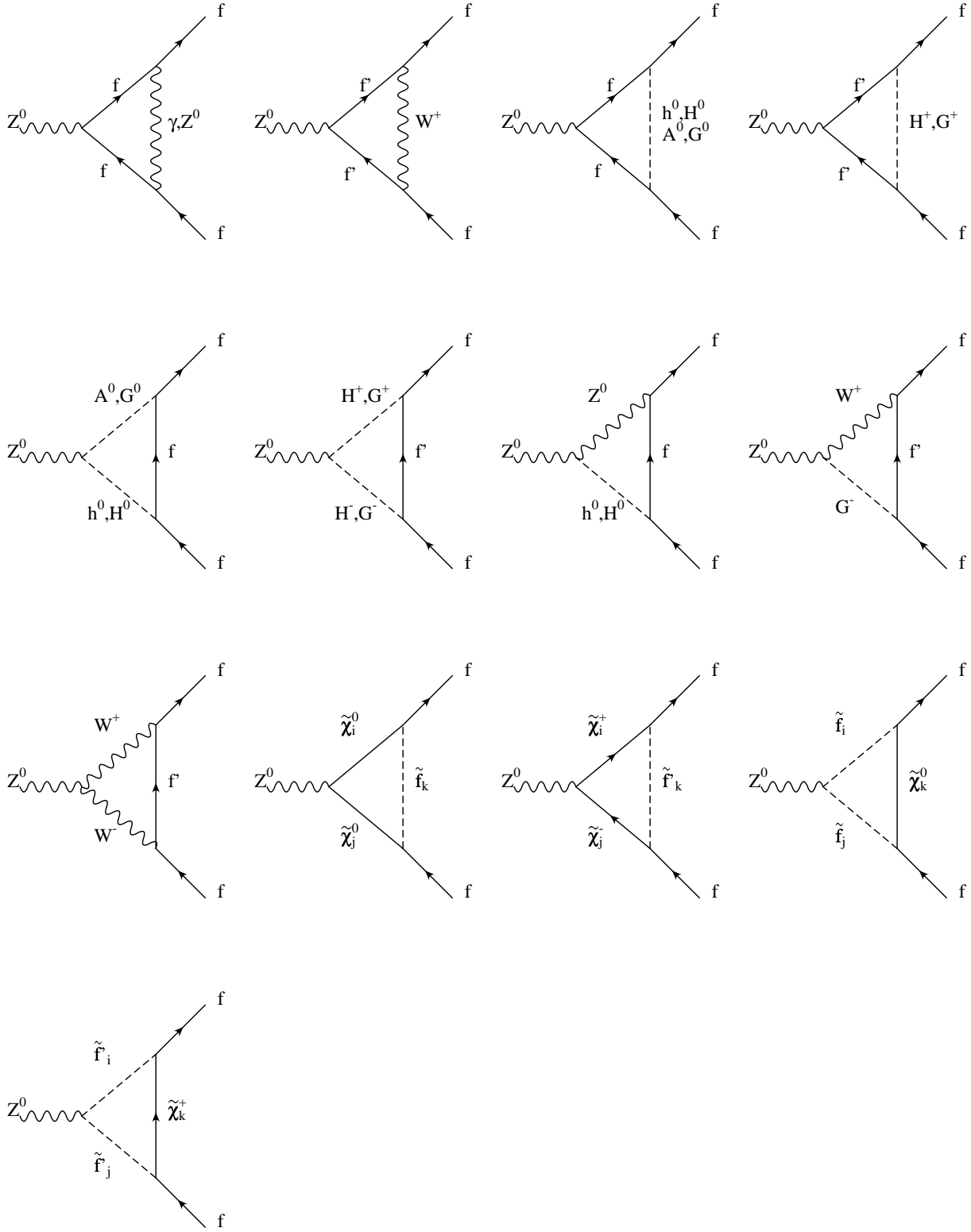


Figure 1: MSSM one-loop $Z \rightarrow f\bar{f}$ vertex correction diagrams. $i, j, k = 1, \dots, 2(4)$ are chargino ($\tilde{\chi}^\pm$), neutralino ($\tilde{\chi}^0$) and sfermions (\tilde{f}) indices, while h, H , are the scalar Higgs bosons, A is the pseudoscalar Higgs boson, and G are Goldstone bosons. No particle permutations are shown.

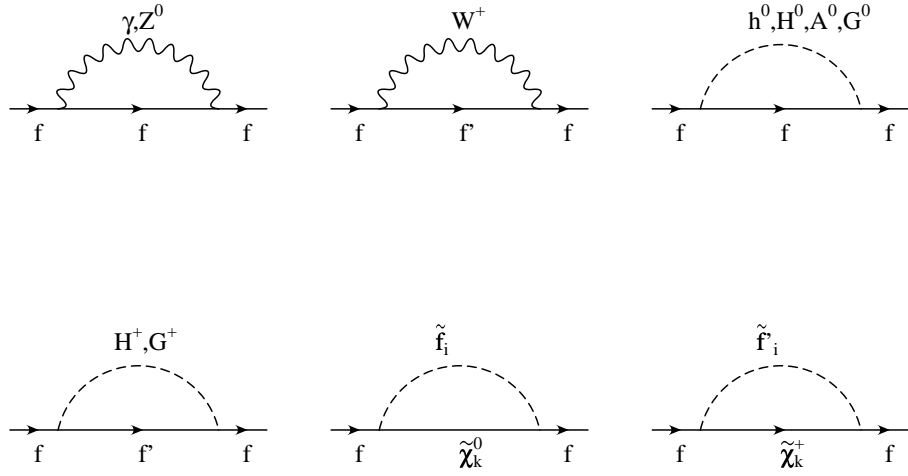


Figure 2: MSSM fermion self-energies. For notation see fig.1.

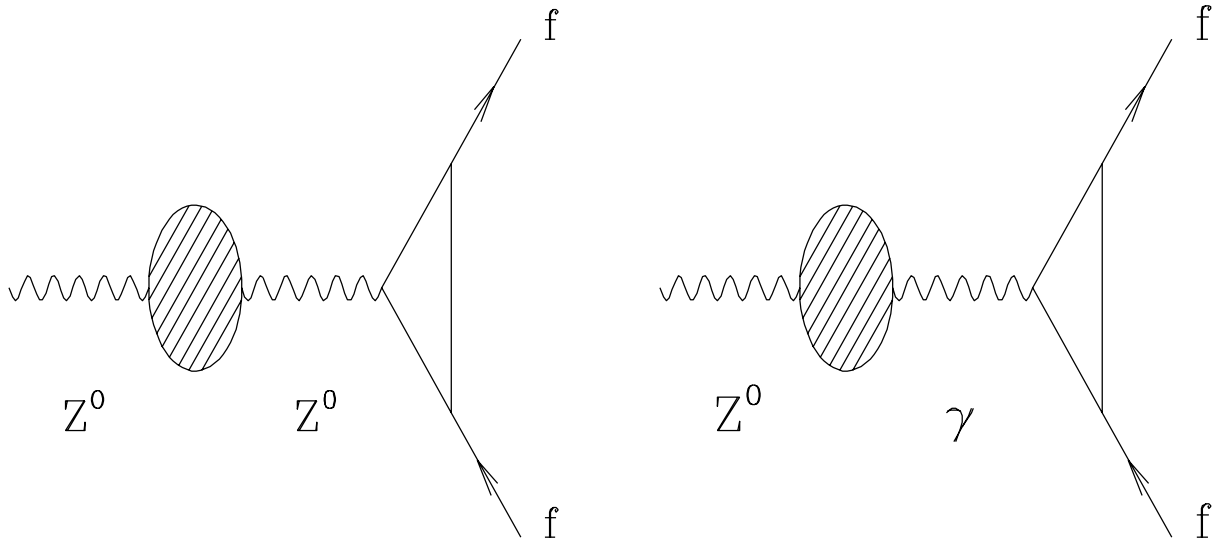


Figure 3: Z boson wave function renormalization. For notation see fig.1.

The non-universal contributions can be written in the following way:

$$\begin{aligned}\Delta v_f &= F_V^{SM} + \Delta F_V, \\ \Delta a_f &= F_A^{SM} + \Delta F_A.\end{aligned}$$

The Standard Model form factors $F_{V,A}^{SM}$ corresponding to the diagrams of figs. 1 and 2 can be found e.g in refs. [30, 27]. The diagrams with a virtual photon are listed for completeness in the figures. They are not part of the effective weak couplings but are treated separately in the QED corrections, together with real photon bremsstrahlung. The non-standard contributions are summarized by

$$\begin{aligned}\Delta F_V &= \sum_i F_V^{(i)} + v_f \delta Z_V^f + a_f \delta Z_A^f \\ \Delta F_A &= \sum_i F_A^{(i)} + v_f \delta Z_A^f + a_f \delta Z_V^f\end{aligned}$$

where the sum extends over the diagrams of fig. 1 with internal charged and neutral Higgs bosons, charginos, neutralinos and scalar fermions. Each diagram contributes

$$F_V^{(i)} \gamma_\mu - F_A^{(i)} \gamma_\mu \gamma_5$$

to the Zff -vertex. The self-energy diagrams of fig. 2 with internal neutral Higgs, chargino, neutralino and sfermion lines determine the field renormalization constants

$$\begin{aligned}\delta Z_V^f &= -\Sigma_V(m_f^2) - 2m_f^2[\Sigma'_V(m_f^2) + \Sigma'_S(m_f^2)] \\ \delta Z_A^f &= \Sigma_A(m_f^2)\end{aligned}\tag{5}$$

with the scalar functions $\Sigma_{V,A,S}$ in the decomposition of the fermion self-energy according to

$$\Sigma = \not{p}\Sigma_V + \not{p}\gamma_5\Sigma_A + m_f\Sigma_S.$$

The contributions from the Higgs sector are given explicitly in ref. [31]. For the genuine SUSY diagrams, the couplings for charginos, neutralinos and sfermions are taken from [32], together with the diagonalization matrices given in the next section.

The universal propagator corrections from the finite Z boson wave function renormalization Z_Z and the γZ mixing Z_M are derived from the (γ, Z) propagator matrix. The inverse matrix is:

$$(\Delta_{\mu\nu})^{-1} = ig_{\mu\nu} \begin{pmatrix} k^2 + \hat{\Sigma}_\gamma(k^2) & \hat{\Sigma}_{\gamma Z}(k^2) \\ \hat{\Sigma}_{\gamma Z}(k^2) & k^2 - M_Z^2 + \hat{\Sigma}_Z(k^2) \end{pmatrix},\tag{6}$$

where $\hat{\Sigma}_\gamma$, $\hat{\Sigma}_Z$, $\hat{\Sigma}_{\gamma Z}$ are the renormalized self energies and mixing. They are obtained by summing the loop diagrams, shown symbolically in fig. 3, and the counter terms and can be found in ref. [13].

The entries in the (γ, Z) propagator matrix:

$$\Delta_{\mu\nu} = -ig_{\mu\nu} \begin{pmatrix} \Delta_\gamma & \Delta_{\gamma Z} \\ \Delta_{\gamma Z} & \Delta_Z \end{pmatrix},\tag{7}$$

are given by:

$$\begin{aligned}
\Delta_\gamma(k^2) &= \frac{1}{k^2 + \hat{\Sigma}_\gamma(k^2) - \frac{\hat{\Sigma}_{\gamma Z}^2(k^2)}{k^2 - M_Z^2 + \hat{\Sigma}_Z(k^2)}} \\
\Delta_Z(k^2) &= \frac{1}{k^2 - M_Z^2 + \hat{\Sigma}_Z(k^2) - \frac{\hat{\Sigma}_{\gamma Z}^2(k^2)}{k^2 + \hat{\Sigma}_\gamma(k^2)}} \\
\Delta_{\gamma Z}(k^2) &= -\frac{\hat{\Sigma}_{\gamma Z}(k^2)}{[k^2 + \hat{\Sigma}_\gamma(k^2)][k^2 - M_Z^2 + \hat{\Sigma}_Z(k^2)] - \hat{\Sigma}_{\gamma Z}^2(k^2)}. \tag{8}
\end{aligned}$$

The renormalization condition to define the mass of the Z boson is given by the pole of the propagator matrix (eq. 6). The pole $k^2 = M_Z^2$ is the solution of the equation:

$$\mathcal{R}e[(M_Z^2 + \hat{\Sigma}_\gamma(M_Z^2))\hat{\Sigma}_Z(k^2) - \hat{\Sigma}_{\gamma Z}^2(M_Z^2)] = 0. \tag{9}$$

Eq. (8) yields the wave function renormalization Z_Z and mixing Z_M :

$$\begin{aligned}
Z_Z &= \text{Res}_{M_Z} \Delta_Z = \frac{1}{1 + \mathcal{R}e \hat{\Sigma}'_Z(k^2) - \mathcal{R}e \left(\frac{\hat{\Sigma}_{\gamma Z}^2(k^2)}{k^2 + \hat{\Sigma}_\gamma(k^2)} \right)'} \Bigg|_{k^2=M_Z^2} \\
Z_M &= -\frac{\hat{\Sigma}_{\gamma Z}(M_Z^2)}{M_Z^2 + \hat{\Sigma}_\gamma(M_Z^2)}. \tag{10}
\end{aligned}$$

2.2 Z boson observables

The fermionic Z boson partial decay widths $\Gamma_{f\bar{f}}$ can be written as follows:

1) $f \neq b$:

$$\begin{aligned}
\Gamma_{f\bar{f}} &= \frac{N_C \sqrt{2} G_\mu M_Z^3}{12\pi} (1 - \Delta r_{MSSM}) \left[(v_{eff}^f)^2 + (a_{eff}^f)^2 \left(1 - \frac{6m_f^2}{M_Z^2}\right) \right] \\
&\quad \cdot \left(1 + \frac{3\alpha_{EM}}{4\pi} Q_f^2\right) (1 + \delta_{QCD}^f), \tag{11}
\end{aligned}$$

where

$$\delta_{QCD}^f = \begin{cases} 0 & , f = \text{leptons} \\ \frac{\alpha_s}{\pi} + 1.405 \left(\frac{\alpha_s}{\pi}\right)^2 - 12.8 \left(\frac{\alpha_s}{\pi}\right)^3 - \frac{Q_f^2 \alpha \alpha_s}{4\pi^2} & , f = \text{quarks} \end{cases}. \tag{12}$$

2) $f = b$:

$$\begin{aligned}
\Gamma_{b\bar{b}} &= \frac{N_C \sqrt{2} G_\mu M_Z^3}{12\pi} (1 - \Delta r_{MSSM}) \left[(v_{eff}^b)^2 + (a_{eff}^b)^2 \right] \\
&\quad \cdot \left(1 + \frac{3\alpha_{EM}}{4\pi} Q_b^2\right) (1 + \delta_{QCD}^b) + \Delta\Gamma_{b\bar{b}}. \tag{13}
\end{aligned}$$

In $\Delta\Gamma_{b\bar{b}}$ the b quark specific finite mass terms with QCD corrections [29] are included. δ_{QCD}^b is given in eq. (12).

The total decay width Γ_Z is the sum of the contributions from leptons and quarks:

$$\Gamma_Z = \sum_f \Gamma_{f\bar{f}} . \quad (14)$$

In the following $\Gamma_{had} = \sum_q \Gamma_{q\bar{q}}$ is the hadronic decay width of the Z boson.

The hadronic peak cross section is defined as

$$\sigma_h = \frac{12\pi}{M_Z^2} \frac{\Gamma_{ee}\Gamma_{had}}{\Gamma_Z^2} . \quad (15)$$

The ratio of the hadronic to the electronic decay width is defined as

$$R_e = \frac{\Gamma_{had}}{\Gamma_{ee}} . \quad (16)$$

The ratio of the partial decay width for $Z \rightarrow b\bar{b}(c\bar{c})$ to the total hadronic decay width is given by

$$R_{b(c)} = \frac{\Gamma_{b\bar{b}(c\bar{c})}}{\Gamma_{had}} . \quad (17)$$

The following quantities and observables depend on the ratio of the vector to axial vector coupling. The effective flavour dependent weak mixing angle can be written as

$$\sin^2 \theta_{eff}^f = \frac{1}{4|Q_f|} \left(1 - \frac{v_{eff}^f}{a_{eff}^f} \right) . \quad (18)$$

The *left-right* asymmetries are given by

$$A_{LR}^f = \mathcal{A}^f = \frac{2v_{eff}^f/a_{eff}^f}{1 + (v_{eff}^f/a_{eff}^f)^2} , \quad (19)$$

while the *forward-backward* asymmetries can be written as

$$A_{FB}^f = \frac{3}{4} \mathcal{A}^e \mathcal{A}^f . \quad (20)$$

3 The MSSM

3.1 Higgs sector

The MSSM has two Higgs doublets:

$$H_1 = \begin{pmatrix} v_1 + \frac{1}{\sqrt{2}} (H^0 \cos \alpha - h^0 \sin \alpha + iA^0 \sin \beta - iG^0 \sin \beta) \\ H^- \sin \beta - G^- \cos \beta \end{pmatrix} \quad (21)$$

$$H_2 = \begin{pmatrix} H^+ \cos \beta + G^+ \sin \beta \\ v_2 + \frac{1}{\sqrt{2}} (H^0 \sin \alpha + h^0 \cos \alpha + iA^0 \cos \beta + iG^0 \sin \beta) \end{pmatrix} \quad (22)$$

Here H, h and A represent the neutral Higgs bosons, while the G 's represent the Goldstone fields, which correspond to the longitudinal polarization components of the heavy gauge bosons. The imaginary and real sectors do not mix, since they have different CP-eigenvalues; α and β are the mixing angles in these different sectors, so one is left with 2 neutral CP-even Higgs bosons H^0 and h^0 , one CP-odd neutral Higgs bosons A^0 , and two charged Higgs bosons.

Their masses are completely determined by the ratio of the vacuum expectation values of $\tan \beta = v_2/v_1$ and the pseudoscalar mass M_A , together with the radiative corrections. The latter ones are taken into account in terms of the effective potential approximation with the leading terms $\sim m_t^4$, including the mixing in the scalar top system [33]. In this way, the coupling constants of the various Higgs particles to gauge bosons and fermions can be taken over from [32] substituting only the scalar mixing angle α by the improved effective mixing angle which is obtained from the diagonalization of the scalar mass matrix, discussed in the next section.

3.2 Sfermion sector

The physical masses of squarks and sleptons are given by the eigenvalues of the 2×2 mass matrix:

$$\mathcal{M}_{\tilde{f}}^2 = \begin{pmatrix} M_{\tilde{Q}}^2 + m_f^2 + M_Z^2(I_3^f - Q_f s_W^2) \cos 2\beta & m_f(A_f + \mu\{\cot \beta, \tan \beta\}) \\ m_f(A_f + \mu\{\cot \beta, \tan \beta\}) & M_{\{\tilde{U}, \tilde{D}\}}^2 + m_f^2 + M_Z^2 Q_f s_W^2 \cos 2\beta \end{pmatrix}, \quad (23)$$

with SUSY soft breaking parameters $M_{\tilde{Q}}, M_{\tilde{U}}, M_{\tilde{D}}, A_f$, and the mass parameter μ from the Higgs sector [1]. It is convenient to use the following notation for the off-diagonal entries in eq. (23):

$$A'_f = A_f + \mu\{\cot \beta, \tan \beta\}. \quad (24)$$

Scalar neutrinos appear only as left-handed mass eigenstates. Up and down type sfermions in (23) are distinguished by setting $f = u$ (d) and select $\cot \beta$ ($\tan \beta$) in the curly brackets. Since the non-diagonal terms are proportional to m_f , it seems natural to assume unmixed sfermions for the lepton and quark case except for the scalar top sector. The \tilde{t} mass matrix is diagonalized by a rotation matrix with a mixing angle Φ_{mix} . Instead of $M_{\tilde{Q}}, M_{\tilde{U}}, M_{\tilde{D}}, A'_t$ for the \tilde{b}, \tilde{t} system the physical squark masses $m_{\tilde{b}_L}, m_{\tilde{b}_R}, m_{\tilde{t}_2}$ can be used together with A'_t or, alternatively, the stop mixing angle Φ_{mix} . For simplicity we assume $m_{\tilde{b}_L} = m_{\tilde{b}_R}$, and $\tilde{u}, \tilde{d}, \tilde{c}, \tilde{s}$ to have masses equal to the \tilde{b} squark mass.

A possible mass splitting between $\tilde{b}_L\text{-}\tilde{t}_L$ yields a contribution to the ρ -parameter⁶ $\rho = 1 + \Delta\rho^0$ in terms of [26]:

$$\Delta\rho_{\tilde{b}\text{-}\tilde{t}}^0 = \frac{3\alpha_{EM}}{16\pi s_W^2 M_W^2} \left(m_{\tilde{b}_L}^2 + m_{\tilde{t}_L}^2 - 2 \frac{m_{\tilde{b}_L}^2 m_{\tilde{t}_L}^2}{m_{\tilde{b}_L}^2 - m_{\tilde{t}_L}^2} \log \frac{m_{\tilde{b}_L}^2}{m_{\tilde{t}_L}^2} \right). \quad (25)$$

As a universal loop contribution, it enters the quantity

$$\Delta r \simeq \Delta\alpha_{EM} - \frac{c_W^2}{s_W^2} \Delta\rho^0 + \dots \quad (26)$$

⁶The superscript in $\Delta\rho^0$ indicates that no left-right mixing is present.

and all the Z boson widths

$$\Gamma_{f\bar{f}} \sim 1 + \Delta\rho^0 + \dots$$

and is thus significantly constrained by the data on M_W and the leptonic widths.

3.3 Chargino/Neutralino sector

The chargino (neutralino) masses and the mixing angles in the gaugino couplings are calculated from μ and the soft breaking parameters M_1, M_2 in the chargino (neutralino) mass matrix[32].

The chargino 2×2 mass matrix is given by

$$\mathcal{M}_{\tilde{\chi}^\pm} = \begin{pmatrix} M_2 & M_W \sqrt{2} \sin \beta \\ M_W \sqrt{2} \cos \beta & -\mu \end{pmatrix}. \quad (27)$$

The physical chargino mass states $\tilde{\chi}_i^\pm$ are the rotated wino and charged Higgsino states:

$$\begin{aligned} \tilde{\chi}_i^+ &= V_{ij} \psi_j^+ \\ \tilde{\chi}_i^- &= U_{ij} \psi_j^- ; \quad i, j = 1, 2. \end{aligned} \quad (28)$$

V_{ij} and U_{ij} are unitary chargino mixing matrices obtained from the diagonalization of the mass matrix eq. 27:

$$U^* \mathcal{M}_{\tilde{\chi}^\pm} V^{-1} = \text{diag}(m_{\tilde{\chi}_1^\pm}, m_{\tilde{\chi}_2^\pm}). \quad (29)$$

The neutralino 4×4 mass matrix can be written as:

$$\mathcal{M}_{\tilde{\chi}^0} = \begin{pmatrix} M_1 & 0 & -M_Z \sin \theta_W \cos \beta & M_Z \sin \theta_W \sin \beta \\ 0 & M_2 & M_Z \cos \theta_W \cos \beta & -M_Z \cos \theta_W \sin \beta \\ -M_Z \sin \theta_W \cos \beta & M_Z \cos \theta_W \cos \beta & 0 & \mu \\ M_Z \sin \theta_W \sin \beta & -M_Z \cos \theta_W \sin \beta & \mu & 0 \end{pmatrix} \quad (30)$$

where the diagonalization can be obtained by the unitary matrix N_{ij} :

$$N^* \mathcal{M}_{\tilde{\chi}^0} N^{-1} = \text{diag}(m_{\tilde{\chi}_i^0}). \quad (31)$$

The elements U_{ij}, V_{ij}, N_{ij} of the diagonalization matrices enter the couplings of the charginos, neutralinos and sfermions to fermions and gauge bosons, as explicitly given in ref. [32]. Note that our sign convention on the parameter μ is opposite to that of ref. [32].

4 Results

The experimental limits included in the fit are summarized in table 1 [7, 8, 9, 10, 11]. They have not been updated with the latest results, since in practice only $R_{b \rightarrow s\gamma}$ and R_b require light SUSY particles, but their deviation from the SM has become so small, that they do not require sparticles below the experimental limits. The experimental observables used in the fits are shown in the first column of table 2. The calculation of the total decay width of

experimental limits	
$m_{\tilde{\chi}_{1,2}^\pm}$	> 65 GeV
$m_{\tilde{\chi}_1^0}$	> 13 GeV
$m_{\tilde{\chi}_2^0}$	> 35 GeV
$m_{\tilde{\chi}_{3,4}^0}$	> 60 GeV
$\Gamma_{Z \rightarrow \text{neutralinos}}$	< 2 MeV
$m_{\tilde{t}_{1,2}}$	> 48 GeV
m_h, m_H, m_A, m_{H^\pm}	> 50 GeV

Table 1: Mass limits assumed for the optimized fits.

the Z boson into neutralinos is based on reference [34], the calculation of the ratio $R_{b \rightarrow s\gamma}$ on reference [35]. The next-to-leading-log calculations increase the SM prediction for $R_{b \rightarrow s\gamma}$ by about 10% to $(3.2 \pm 0.5)10^{-4}$ [24]. This higher order contribution was taken into account in the first order calculation by choosing the renormalization scale $\mu = 0.7 \cdot m_b$.

As discussed in section 2.1, R_b depends on stop -, chargino- and Higgs masses. First the behaviour of the chargino masses as a function of the SUSY parameters μ and M_2 is discussed, then the R_b dependence on the relevant SUSY masses is studied, both for the low and high $\tan\beta$ scenarios. These studies are followed by the best solutions in the SM and MSSM.

4.1 Chargino Masses

In order to explain an enhanced value of R_b in the data, the MSSM needs a light right handed stop and light chargino (low $\tan\beta$ scenario), or a light pseudoscalar Higgs A (high $\tan\beta$ scenario) [15]-[23]. A higgsino-like chargino can be obtained for a low value of the parameter μ in the mass matrix (eq. 27). Figs. 4 and 5 show the dependence of the chargino masses on the parameter μ . For high $\tan\beta$, $m_{\tilde{\chi}_2}$ is almost symmetric around $\mu = 0$, whereas for low $\tan\beta$ this dependence is more complicated, as can be seen from fig. 4. For $M_2 = 3|\mu|$ the light chargino mass passes zero at $\mu = -40$ GeV, so the following low $\tan\beta$ plots were made for $\mu > -40$ GeV and $\mu \leq -40$ GeV. The asymmetric structure of fig. 4 is reflected in the contours of constant R_b in the $m_{\tilde{\chi}_2}$ versus light scalar top $m_{\tilde{t}_2}$ plane (see fig. 6). Values of R_b up to 0.2194 are possible (see figs. 6 and 7), although these special regions of the parameter space are already experimentally excluded by the lower limits on sparticle masses.

For $M_2 = 3|\mu|$ the lightest chargino is mostly higgsino-like, while the heavier one is gaugino like. Mixing the charginos more by taking $M_2 = |\mu|$ does not change these results very much, as can be seen from a comparison of the χ^2 distributions in fig. 8 ($M_2 = 3|\mu|$) and fig. 9 ($M_2 = |\mu|$). The small increase of the χ^2 at chargino masses around 80 GeV in the left hand part of fig. 9 is due to neutralino threshold singularities, for which an additional χ^2 contribution has been added, when the sum of two neutralino masses is close to the Z^0 mass. The sharp increase of the χ^2 function at low chargino masses is due to experimental limits on chargino, neutralino and stop masses from LEP 1.5 [7, 8, 9].

4.2 Low $\tan\beta$ scenario

Fig. 10 shows the change in the best obtainable χ^2 in the chargino - stop plane. For each value of the lighter scalar top $m_{\tilde{t}_2}$ and lighter chargino $m_{\tilde{\chi}_2^\pm}$ in a grid of 10×10 points an optimization of m_t , α_s and the stop mixing angle Φ_{mix} was performed, assuming $M_2 = 3|\mu|$ for a fixed value of $\tan\beta = 1.6$. In the next section this assumption on M_2 will be dropped. Low sparticle masses yield a sharp increase in the $\Delta\chi^2$ in fig. 10 because of the included mass limits. The minimum χ^2 is obtained for chargino masses above 80 GeV and increases only slowly with increasing sparticle masses. R_b increases significantly with decreasing values of the stop and chargino mass, as can be seen from fig. 11. Much less significant is the change of R_c . Within the plane of fig. 11 it changes less than 0.0005 units. The increase of R_b must be compensated by a decrease of α_s (see fig. 12) in order to keep the total Z^0 -width constant. The stop mixing angle Φ_{mix} , shown in fig. 13, is mainly determined by the CLEO measurement of $R_{b \rightarrow s\gamma}$. The chargino contribution to $R_{b \rightarrow s\gamma}$ is proportional to the Higgs mixing parameter μ , which changes its sign for $m_{\tilde{\chi}^\pm} \approx 60$ GeV (see fig.4), so the $R_{b \rightarrow s\gamma}$ rate changes rapidly for these chargino masses, as shown in fig. 14.

4.3 High $\tan\beta$ scenario

Similar fits can be performed for the high $\tan\beta$ scenario in the pseudoscalar Higgs m_A versus light chargino plane. In fig. 15 the resulting change in the χ^2 is given for fixed $\tan\beta = 35$. For small chargino masses there is a sharp increase in the χ^2 due to the corresponding mass limit, see above. The highest values for R_b can be obtained for small values of m_A and $m_{\tilde{\chi}^\pm}$, see fig. 16. As in the low $\tan\beta$ case the enhancement of R_b must be compensated by a decrease of α_s , see fig. 17, and the change of R_c is small, less than 0.0006 within the given parameter plane. The mixing angle, shown in fig. 18, is mainly determined by the $R_{b \rightarrow s\gamma}$ rate, which can be fitted in the whole m_A - $m_{\tilde{\chi}^\pm}$ plane, see fig. 19.

4.4 Best Solutions

Standard Model Fits:

The predictions of the SM are completely determined by the set of six input parameters M_Z , m_t , the SM Higgs mass M_h , α_s , α_{EM} and G_μ . The error of the muon decay constant is so small that G_μ can be treated as a fixed parameter. The fine structure constant was taken to be $1/\alpha(M_Z) = 128.89 \pm 0.09$ [36]. The error on $1/\alpha(M_Z)$ turns out not to be negligible: fixing $1/\alpha(M_Z)$ underestimates the error on the Higgs mass by $\approx 30\%$. The SM predictions were obtained from the ZFITTER package [12] and all the error correlations were taken from [4]. The fits were made with M_Z , m_t , m_H , α_s and α as free parameters, which resulted in

$$\begin{aligned}
 M_Z &= 91.186 \pm 0.002 \text{ GeV} \\
 m_t &= 172.0_{-5.7}^{+5.8} \text{ GeV} \\
 m_H &= 141_{-77}^{+140} \text{ GeV} \\
 \alpha_s(M_Z) &= 0.1197 \pm 0.0031 \\
 1/\alpha(M_Z) &= 128.90_{-0.090}^{+0.089}
 \end{aligned}$$

The minor differences to the results given in [4] originate from the inclusion of the $R_{b \rightarrow s\gamma}$ ratio. The electroweak mixing angle can be determined from these parameters:

$$\sin^2 \theta_{\overline{MS}} = 0.2316 \pm 0.0004.$$

Both the strong coupling constant and the electroweak mixing angle $\sin^2 \theta_{\overline{MS}}$ have been determined at the scale M_Z in the \overline{MS} renormalization scheme. With $m_t = 175$ GeV $\sin^2 \theta_{\overline{MS}} = \sin^2 \theta_{eff}^{lept}$ to an accuracy better than 0.0001. The quoted errors have been determined using MINOS [14]. Further details of the procedure are described elsewhere, see for example [37, 38]. The $\chi^2/d.o.f$ of the SM fit is 19.6/15 which corresponds to a probability of 19%. Here, the main contributions to the χ^2 originate from $\sin^2 \theta_{eff}^{lept}$ from SLD ($\Delta\chi^2 = 4.9$), R_b ($\Delta\chi^2 = 3.1$) and A_{FB}^b ($\Delta\chi^2 = 3.5$). The prediction of R_c is good. If $R_{b \rightarrow s\gamma}$ is excluded from the fit, one obtains a $\chi^2/d.o.f$ of 18.9/14, corresponding to a probability of 17%, in agreement with [4]. The correlation parameter between m_H and m_t for the best fit is approximately 0.7; this strong correlation is shown in fig. 20. One observes that the upper limit on the Higgs mass is obtained for m_t above 175 GeV; however, the upper limit is sensitive to $\sin^2 \theta_{eff}^{lept}$ as shown by the dashed contour in fig. 20, where the precise value of $\sin^2 \theta_{eff}^{lept}$ from SLD was excluded from the fit. The dependence of $\sin^2 \theta_{eff}^{lept}$ on the SM Higgs mass is approximately logarithmic (see fig. 21). The LEP data without SLD yields $m_H = 241_{-123}^{+218}$ GeV, while the SLD value of $\sin^2 \theta_{eff}^{lept}$ corresponds to $m_H = 16_{-9}^{+16}$ GeV; both m_h values are indicated in figure 21 (by the square and the circle, respectively). The SLD value is excluded by the lower limit of 58.4 GeV from the combined LEP experiments [11], so more data is eagerly awaited.

The $\Delta\chi^2$ dependence of the Higgs mass is shown in fig. 22 for various conditions. Clearly, the $\sin^2 \theta_{eff}^{lept}$ from SLD gives a large weight, while the new value from R_b plays only in minor role in contrast to the previous value[5].

MSSM Fits and Comparison with the SM:

In order to obtain the best MSSM fits the assumption $M_2 = 3|\mu|$ is dropped and M_2 is treated as a free parameter. As discussed in section 2.1 the dominant contributions vary for the high and the low $\tan \beta$ scenario. The preferred $\tan \beta$ values for these scenarios are around 35 and 1.6, respectively. Since the fit is not very sensitive to the precise $\tan \beta$ value, it was fixed to these values. The fitted MSSM parameters and the corresponding SUSY masses are given in table 3; the predicted values of all observables and their pulls are summarized in table 2. For the MSSM M_Z , G_μ and α were treated as fixed parameters because of their small errors compared with the uncertainties from the other parameters. The MSSM prediction of the W-boson mass is always higher than the SM one, but the values of the strong coupling constant, the electroweak mixing angle and the top mass are very similar in the MSSM:

$$\begin{aligned} \alpha_s(M_Z) &= 0.116 \pm 0.005 \\ m_t &= 172 \pm 5 \text{ GeV} \\ \sin^2 \theta_{\overline{MS}} &= 0.2315 \pm 0.0004. \end{aligned}$$

These values are for the low $\tan\beta$ scenario, but for high $\tan\beta$ the same values are obtained, except for $\alpha_s = 0.119 \pm 0.005$ in that case. The remaining parameters are given in table 3. A direct comparison to the SM fits is given in figs. 24-25. The SM fit to the 20 measurements of table 2 with 5 parameters yields $\chi^2/d.o.f. = 19.6/15$ which corresponds to a probability of 19%, while the MSSM fits correspond to probabilities of 17% ($\tan\beta = 1.6$, $\chi^2/d.o.f. = 16.6/12$) and 11% ($\tan\beta=35$, $\chi^2/d.o.f. = 18.1/12$). In counting the d.o.f the insensitive (and fixed) parameters are ignored, so only the parameters given in table 3 are considered. The difference in χ^2 between SM and MSSM fits is mainly caused by R_b , which is better described in the MSSM, although the difference in χ^2 is insufficient to distinguish between the models.

The Higgs mass is not an independent parameter in the MSSM, since the couplings in the Higgs potential are gauge couplings, which limit the mass of the lightest Higgs to a rather narrow range[39]. The high $\tan\beta$ needs a light pseudoscalar Higgs mass. As the lightest Higgs mass is strongly correlated with the pseudoscalar Higgs mass, it is also low. Similar Higgs values in the MSSM model were obtained in ref. [40].

An interesting point is the fitted value of $\alpha_s(M_Z)$. In previous analysis with the high values of R_b , $\alpha_s(M_Z)$ in the MSSM (≈ 0.11) was always significantly smaller than the SM value (0.123 ± 0.005 [11]), which supported the low energy values from deep inelastic scattering (DIS) (0.112 ± 0.005 [11]) and lattice calculations of the heavy quark splittings (0.110 ± 0.006 [11]). However, the discrepancies between the low energy α_s values and the LEP data have practically disappeared at the Warsaw Conference[41]: the Standard Model value (0.120 ± 0.003 , see above) is now in agreement with DIS measurements (0.115 ± 0.005 [41]), lattice calculations 0.117 ± 0.003 [41] and the world average 0.118 ± 0.003 [41]. The MSSM values of α_s are in good agreement with these other determinations, as shown in fig. 26.

The particle spectrum for the best fits, as shown in table 3, suggests that some SUSY particles could be within reach of LEP II. Unfortunately, if the stop-, chargino- and/or Higgs mass are well above the discovery reach of LEP II, the χ^2 of the fit increases at most up to the SM value, since these particles basically decouple as soon as they become heavier than the heaviest SM mass, say the top mass of about 200 GeV. So one cannot get upper limits on these particles, since the probability changes only a few percent between the SM and MSSM.

5 CMSSM and R_b

In the MSSM fits discussed above the lightest stop is mainly right-handed, while the left-handed stop has to be heavy. If both would be light, then all other squarks would likely be light, which would upset the good agreement between the SM and all other electroweak data. A large mass splitting in the stop sector needs a very artificial fine tuning of the few free parameters in the Constrained MSSM, which assumes unification of gauge and b- τ Yukawa couplings[38]. This is obvious from the sfermion mixing matrix for the stop quarks, eq. 23. The D-terms proportional to $\cos 2\beta$ are negligible for $\tan\beta \approx 1$. If one of the diagonal elements is much larger than m_t , the off-diagonal terms of the order m_t will not cause a mixing and the difference between the left- and right-handed stops has to come from the

evolution of the diagonal terms (for the notation see ref. [38]):

$$\begin{aligned} \frac{dM_{\tilde{Q}_3}^2}{dt} &= \left(\frac{16}{3}\tilde{\alpha}_3 M_3^2 + 3\tilde{\alpha}_2 M_2^2 + \frac{1}{15}\tilde{\alpha}_1 M_1^2 \right) \\ &\quad - [Y_t(M_{\tilde{Q}_3}^2 + M_{\tilde{U}_3}^2 + m_{H_2}^2 + A_t^2 m_0^2) \\ &\quad + Y_b(M_{\tilde{Q}_3}^2 + M_{\tilde{D}_3}^2 + m_{H_1}^2 + A_b^2 m_0^2)] \end{aligned} \quad (32)$$

$$\begin{aligned} \frac{dM_{\tilde{U}_3}^2}{dt} &= \left(\frac{16}{3}\tilde{\alpha}_3 M_3^2 + \frac{16}{15}\tilde{\alpha}_1 M_1^2 \right) \\ &\quad - 2Y_t(M_{\tilde{Q}_3}^2 + M_{\tilde{U}_3}^2 + m_{H_2}^2 + A_t^2 m_0^2) \end{aligned} \quad (33)$$

One observes that the difference between left- and right handed stops, denoted by \tilde{Q}_3 and \tilde{U}_3 , respectively), depends on the Yukawa couplings for top and bottom (Y_t, Y_b) and the trilinear couplings $A_{t(b)}$. For low $\tan\beta$ Y_b is negligible, while A_t and Y_t are not free parameters, since they go to fixed point solutions[38]. Therefore there is little freedom to adjust these parameters within the CMSSM in order to get a large splitting between the left- and right-handed stops.

In addition, problems arise with electroweak symmetry breaking, since this requires the Higgs mixing parameter μ to be much heavier than the gaugino masses[38], while R_b requires low values of μ for a significant enhancement (since the chargino has to be preferably Higgsino-like). In conclusion, within the CMSSM an enhancement of R_b above the SM is practically excluded.

6 Conclusions

Both the MSSM and SM provide a good description of all electroweak data. The best $\chi^2/d.o.f$ in the MSSM (SM) is 16.6/12 (19.6/15), which corresponds to a probability of 17% (19%). The lower χ^2 of the MSSM is mainly due to the better description of R_b , but the fit requires an unnatural large splitting in the stop sector, as discussed in the previous section. Since the final analysis of most of the available LEP data is still in progress, one has to wait and see if the present preliminary value of R_b will indeed stay above the SM prediction.

Symbol	measurement	best fit observables					
		SM		MSSM			
$\tan\beta$ and pull			pull	1.6	pull	35	pull
M_Z [GeV]	91.1863 ± 0.0020	91.1861	0.08	91.1863	-	91.1863	-
Γ_Z [GeV]	2.4946 ± 0.0027	2.4958	-0.45	2.4946	-0.00	2.4940	0.22
σ_h [nb]	41.508 ± 0.056	41.468	0.72	41.461	0.84	41.449	1.05
R_l	20.778 ± 0.029	20.755	0.80	20.769	0.32	20.772	0.22
A_{FB}^l	0.0174 ± 0.0010	0.0160	1.41	0.0162	1.20	0.0162	1.22
R_b	0.2178 ± 0.0011	0.2158	1.75	0.2174	0.38	0.2168	0.92
R_c	0.1715 ± 0.0056	0.1722	-0.13	0.1707	0.14	0.1708	0.12
A_{FB}^b	0.0979 ± 0.0023	0.1022	-1.87	0.1031	-2.26	0.1031	-2.24
A_{FB}^c	0.0735 ± 0.0048	0.0731	0.10	0.0736	-0.02	0.0736	0.01
\mathcal{A}_b	0.863 ± 0.049	0.933	-1.45	0.9353	-1.49	0.9356	-1.50
\mathcal{A}_c	0.625 ± 0.084	0.667	-0.50	0.6678	-0.51	0.668	-0.51
\mathcal{A}_τ	0.1401 ± 0.0067	0.1460	-0.88	0.1470	-1.03	0.1466	-0.97
\mathcal{A}_e	0.1382 ± 0.0076	0.1460	-1.03	0.1470	-1.16	0.1469	-1.14
$\sin^2 \theta_{eff}^{lept}(Q_{FB})$	0.2320 ± 0.0010	0.2316	0.35	0.2315	0.48	0.2315	0.46
M_W [GeV]	80.356 ± 0.125	80.355	0.01	80.403	-0.38	80.428	-0.58
$1 - M_W^2/M_Z^2$	0.2244 ± 0.0042	0.2235	0.23	0.2225	0.45	0.2220	0.56
m_t [GeV]	$175 \pm 6.$	172.0	0.50	172.5	0.42	172.0	0.50
$\sin^2 \theta_{eff}^{lept}(A_{LR})$	0.23061 ± 0.00047	0.2316	-2.21	0.2315	-1.94	0.2315	-1.97
$R_{b \rightarrow s\gamma}/10^{-4}$	$2.32 \pm 0.67 \pm 0.5$	3.1	-0.86	2.43	-0.12	2.33	0.0
$1/\alpha(M_Z)$	128.896 ± 0.09	128.905	-0.10	128.89	-	128.89	-

Table 2: Measurements[4] and the predicted results of the fits with minimum χ^2 . The pulls are defined by (measurement - predicted value) / error of the measurement. The second error for $R_{b \rightarrow s\gamma}$ has been added to take care of the uncertainty by the renormalization scale used for the calculation of that quantity. For the MSSM fits M_Z and $1/\alpha(M_Z)$ were taken as fixed parameters, because their uncertainties are negligible compared to uncertainties arising from the soft breaking parameters. Leaving them free does not change the results.

Fitted SUSY parameters and masses		
Symbol	$\tan \beta=1.6$	$\tan \beta=35$
m_t [GeV]	172	172
α_s	0.116	0.1190
M_2 [GeV]	113	-
μ [GeV]	60	111
$m_{\tilde{t}_2}$ [GeV]	48	187
ϕ_{mix}	-0.18	0.04
m_A [GeV]	-	50
Particle Spectrum		
$m_{\tilde{t}_1}$ [GeV]	≈ 1 TeV	
$m_{\tilde{t}_2}$ [GeV]	48	187
$m_{\tilde{q}}$ [GeV]	1 TeV	
$m_{\tilde{l}}$ [GeV]	0.5 TeV	
$m_{\tilde{\chi}_1^\pm}$ [GeV]	149	1504
$m_{\tilde{\chi}_2^\pm}$ [GeV]	84	111
$m_{\tilde{\chi}_1^0}$ [GeV]	54	107
$m_{\tilde{\chi}_2^0}$ [GeV]	64	114
$m_{\tilde{\chi}_3^0}$ [GeV]	100	722
$m_{\tilde{\chi}_4^0}$ [GeV]	150	1504
m_h [GeV]	109	50
m_H [GeV]	≈ 1.5 TeV	112
m_A [GeV]	1.5 TeV	50
m_{H^\pm} [GeV]	≈ 1.5 TeV	123
$\chi^2/d.o.f.$	16.6/12	18.1/12
Probability	17%	11%

Table 3: Values of the fitted parameters (upper part) and corresponding mass spectrum (lower part). On the right hand side the results of the optimization for high $\tan \beta$ are given. The dashes indicate irrelevant parameters which were chosen high.

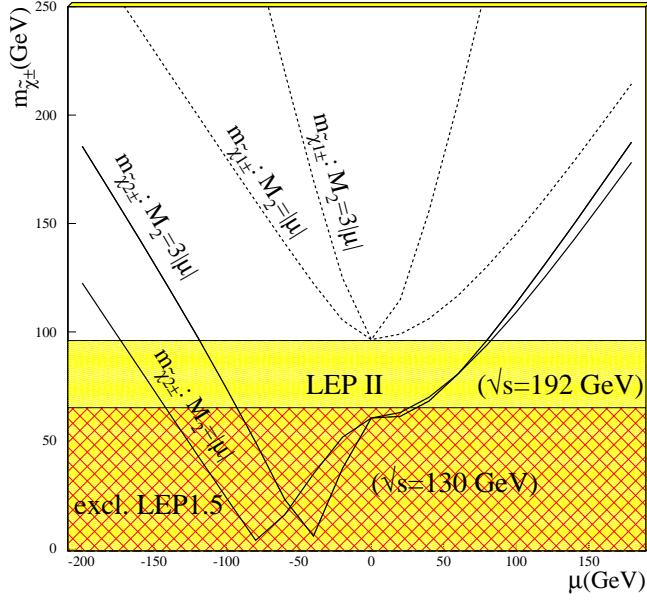


Figure 4: Dependence of the chargino masses (solid line=lightest one) on the parameter μ for $M_2 = |\mu|$ and $M_2 = 3|\mu|$ for $\tan\beta = 1.6$, $\alpha_s \approx 0.117$ and $m_{\tilde{t}_2} \approx 60$ GeV. The shaded regions indicate chargino masses less than 65 GeV which are excluded by *LEP* 1.5 and chargino masses less than 96 GeV, which is the discovery reach for *LEP* II. Note that two light charginos are easier obtained, if $\mu \approx M_2$.

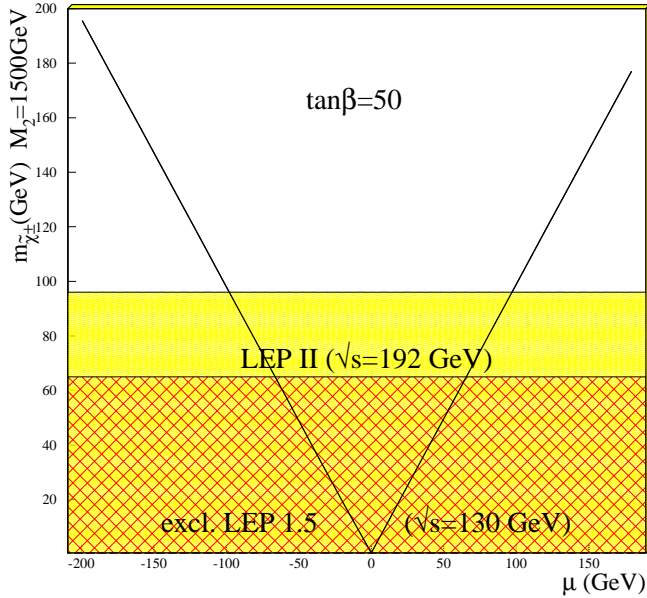


Figure 5: Dependence of the lightest chargino mass on the parameter μ for $\tan\beta = 35$ and $M_2=1500$ GeV. The shaded regions as in fig. 4. The heavy chargino mass is close to $M_2 = 1500$ GeV(not indicated).

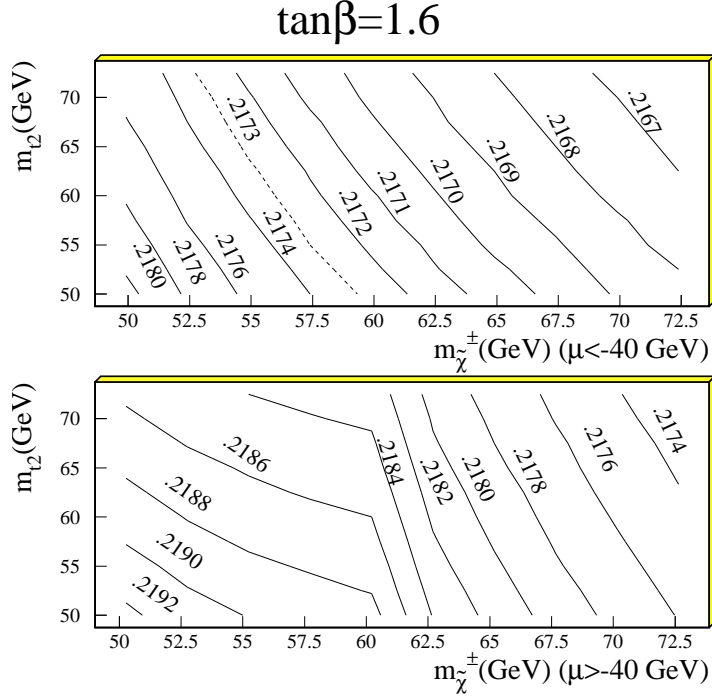


Figure 6: R_b in the light stop versus light chargino plane with $M_2 = 3|\mu|$ and $\tan\beta = 1.6$. The upper part shows the solution with $\mu < -40$ GeV, in the lower part the one with $\mu > -40$ GeV is displayed. In the latter solution quite high values for R_b are possible, as can be seen in the figure. The dashed line in the upper plot indicates the old 2σ lower limit of R_b . Recent updates of electroweak data yield $R_b = 0.2178 \pm 0.0011$.

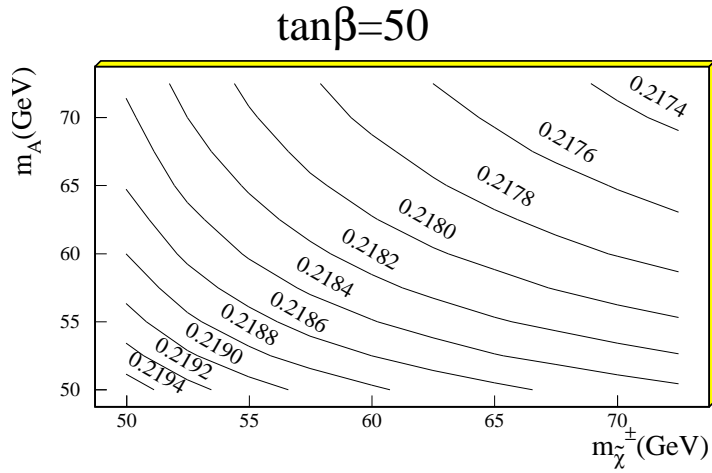


Figure 7: R_b in the m_A versus light chargino plane with $M_2 = 3|\mu|$ for the high $\tan\beta$ solution. μ was chosen positive here. In this case choosing the opposite sign for μ doesn't change R_b .

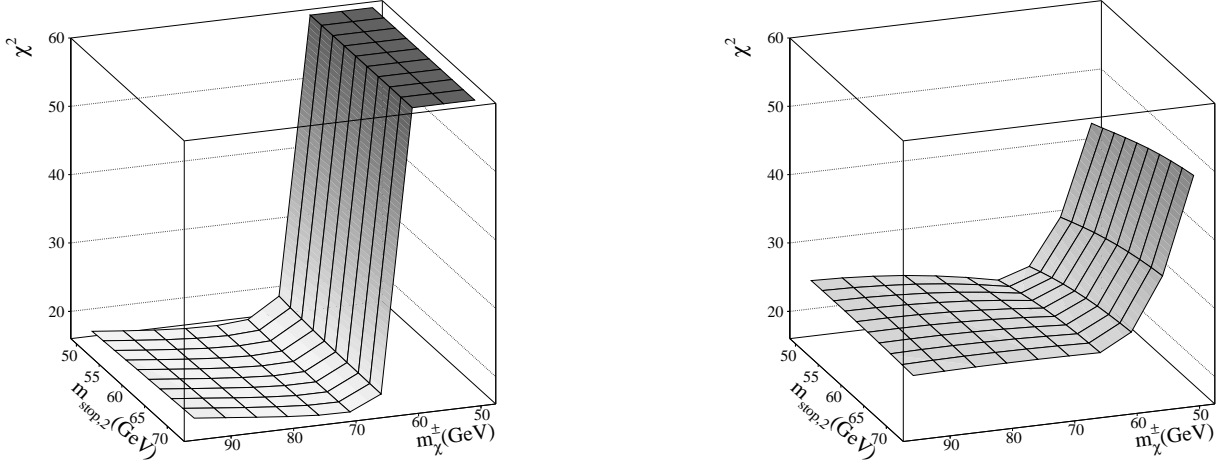


Figure 8: Dependence of the absolute χ^2 for $\mu > -40$ GeV (left side) and $\mu < -40$ GeV (right side), using $M_2 = 3|\mu|$. No optimization of parameters was performed, but they were fixed to values near the minimum.

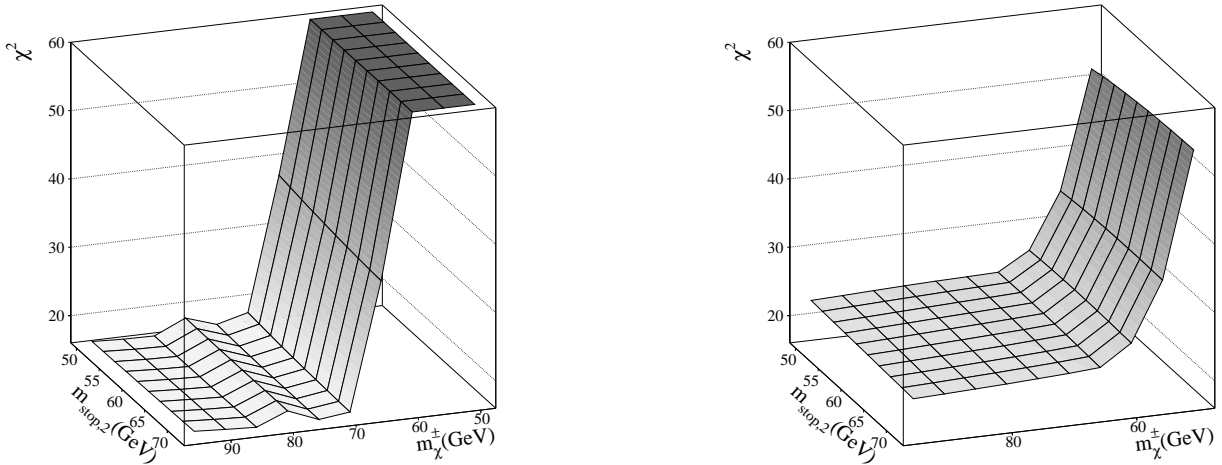


Figure 9: The same as 8, but for $M_2 = |\mu|$.

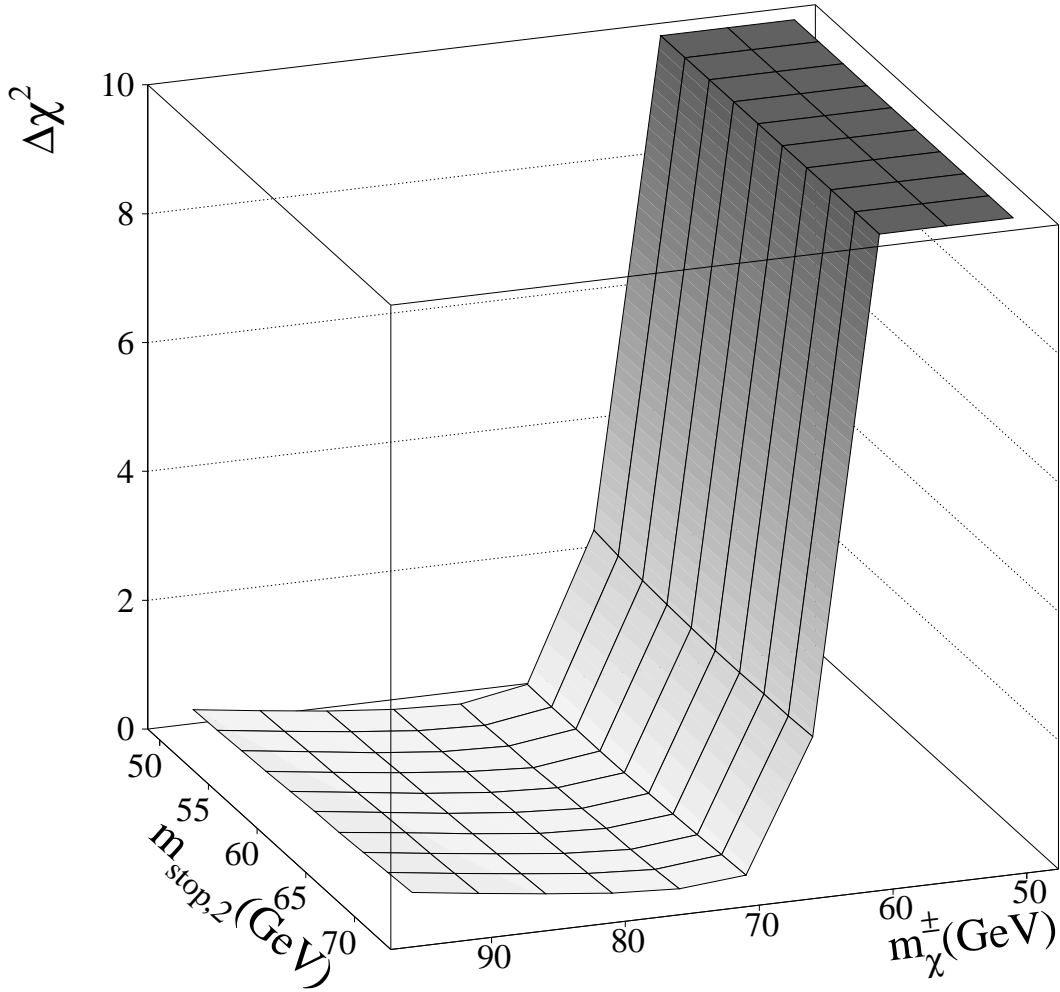


Figure 10: The $\Delta\chi^2$ in the light stop and light chargino plane for $\tan\beta = 1.6$. At each point of the grid an optimization of m_t , α_s and the stop mixing angle ϕ_{mix} was performed with $\mu > -40$ GeV and $M_2 = 3|\mu|$.

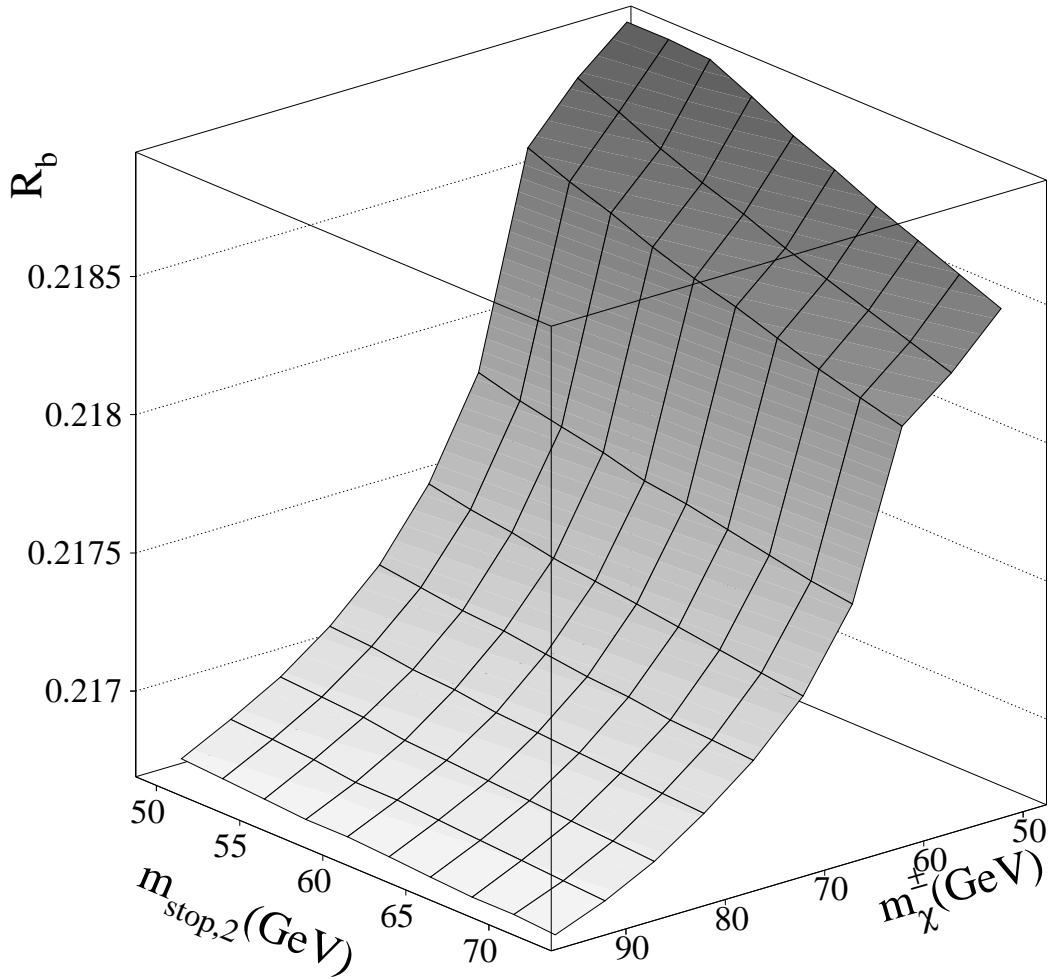


Figure 11: R_b in the light stop and light chargino plane. Optimization as in fig. 10.

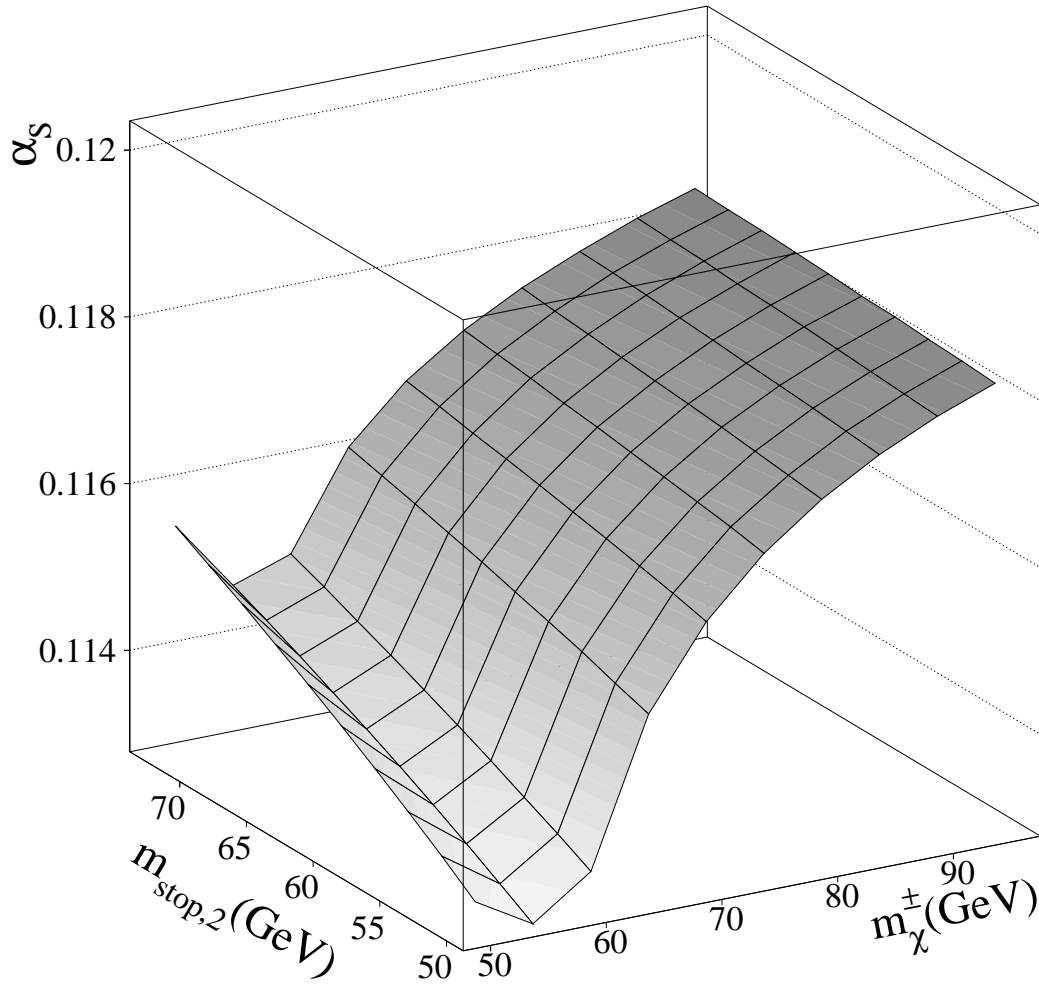


Figure 12: α_s in the light stop and light chargino plane. Optimization as in fig. 10.

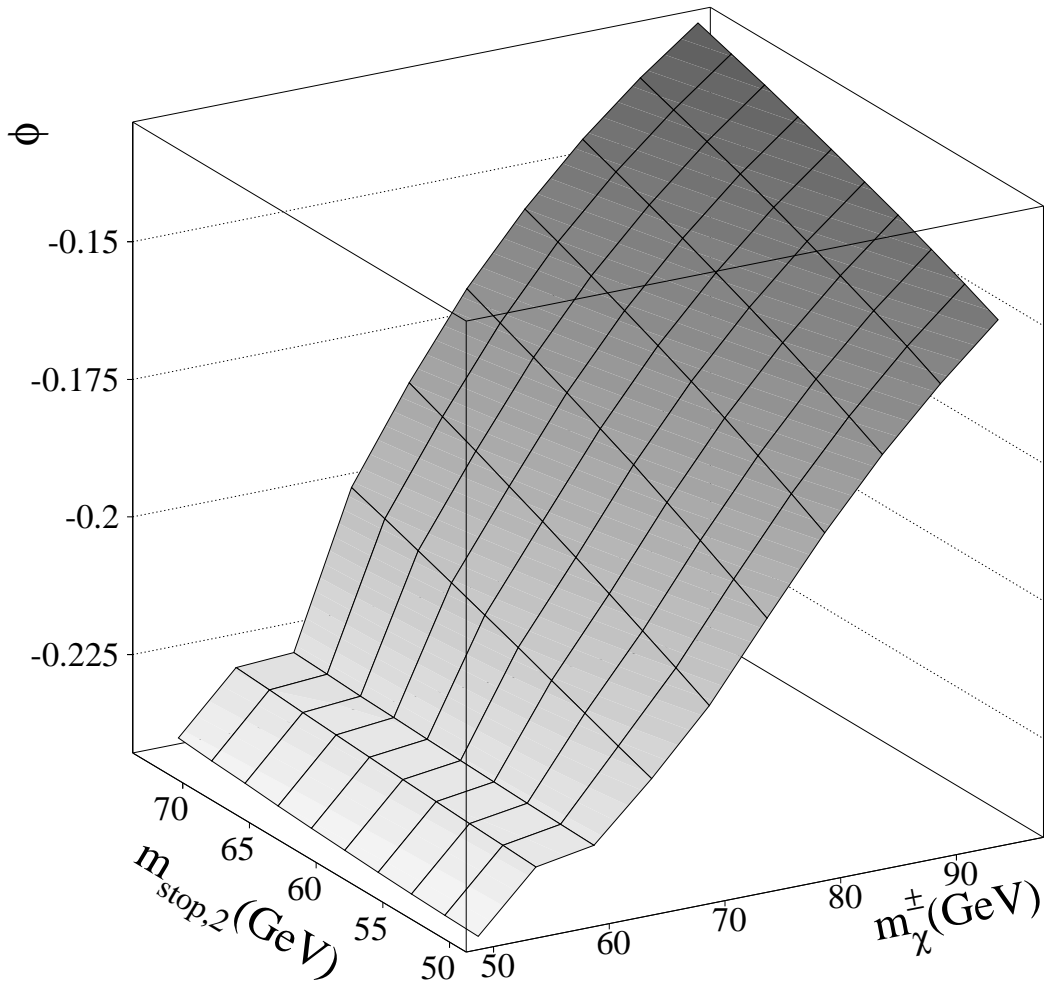


Figure 13: Stop mixing angle ϕ_{mix} in the light stop and light chargino plane. It is mainly determined by the $R_{b \rightarrow s\gamma}$ rate. Optimization as in fig. 10.

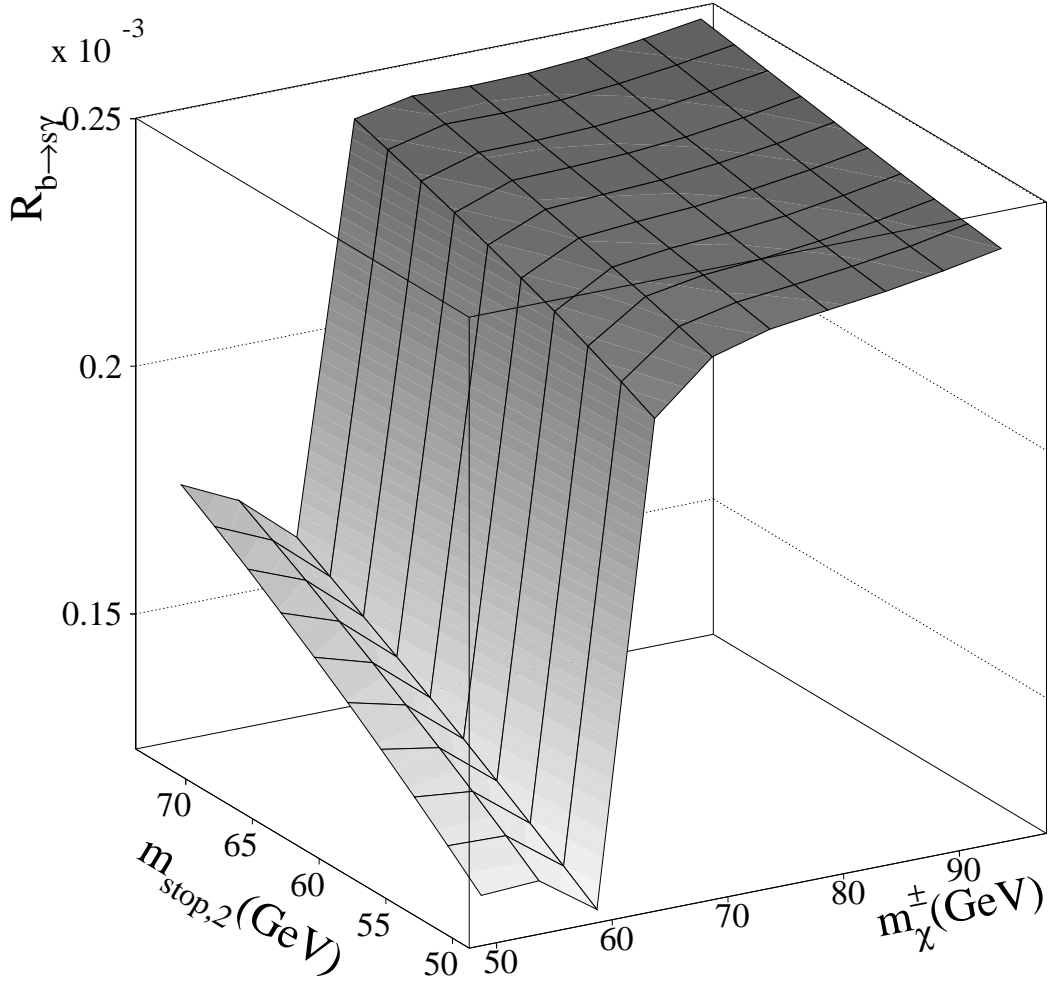


Figure 14: $R_{b \rightarrow s \gamma}$ in the light stop and light chargino plane for $\tan \beta = 1.6$. For chargino masses higher than 60 GeV (and $\mu > 0$) the predicted value is close to the CLEO measurement of $2.32 \pm 0.67 \times 10^{-4}$. Optimization as in fig. 10.

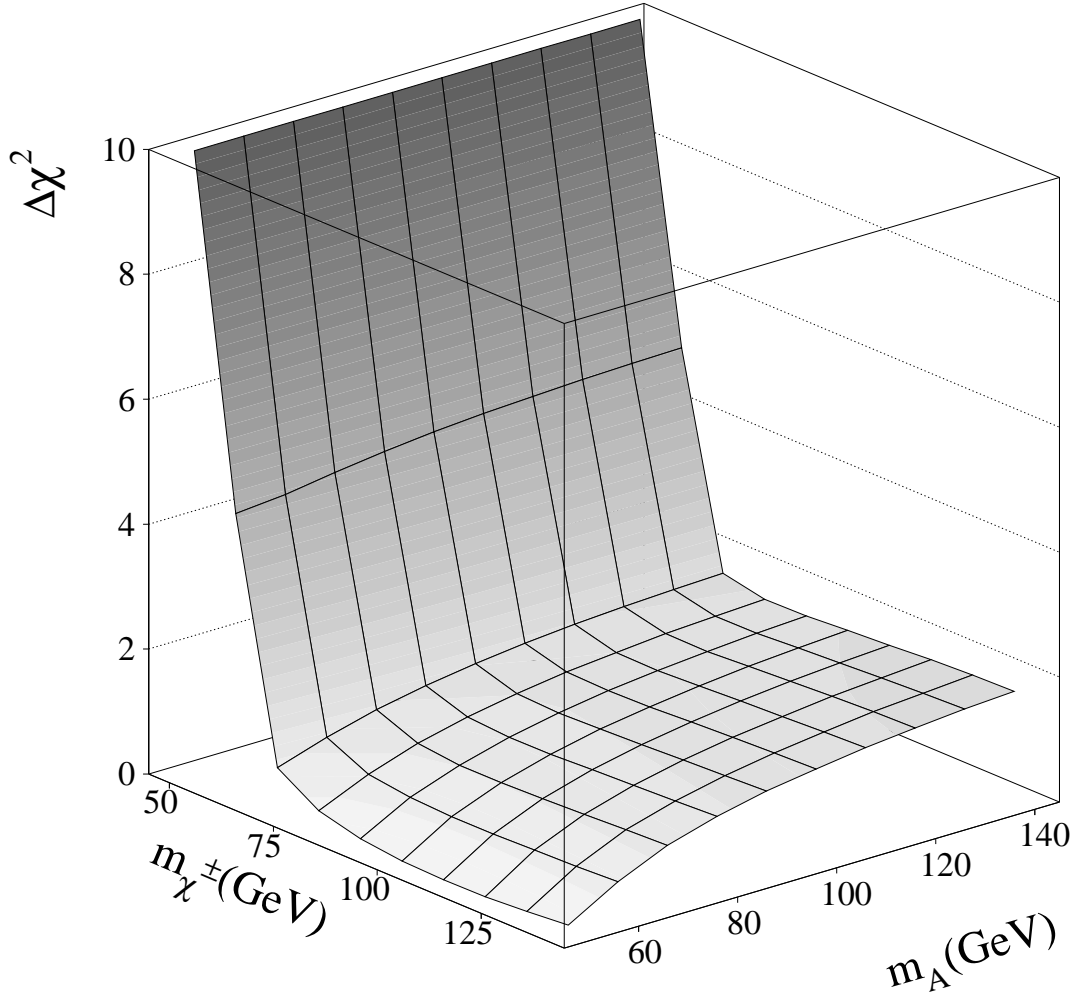


Figure 15: The $\Delta\chi^2$ in the pseudoscalar Higgs and light chargino plane for $\tan\beta = 35$. For each given m_A and light chargino mass an optimization of m_t , α_s , $m_{\tilde{t}_2}$ and the stop mixing angle ϕ_{mix} was performed. The irrelevant parameter M_2 was set to 1500 GeV.

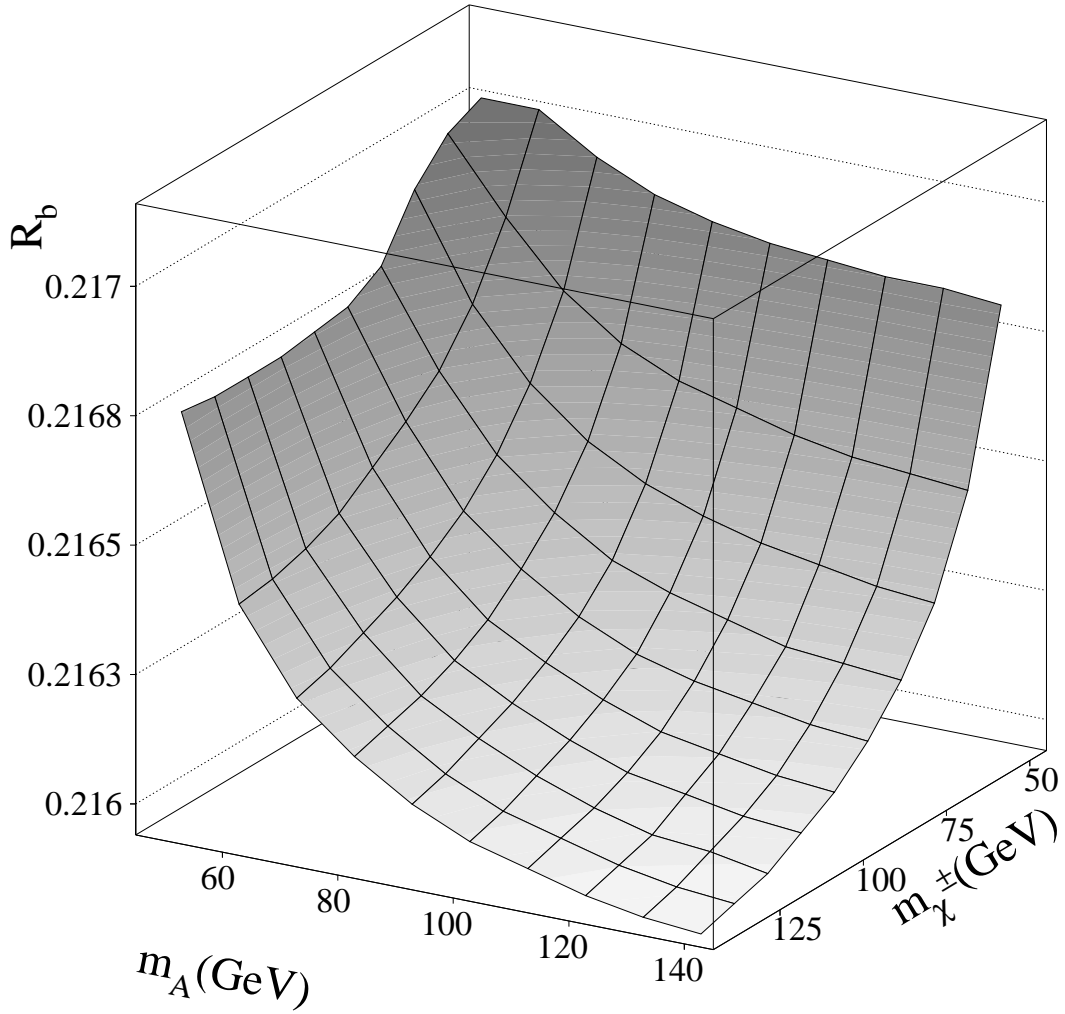


Figure 16: R_b in the pseudoscalar Higgs and light chargino plane for $\tan \beta = 35$. Optimization as in fig. 15.

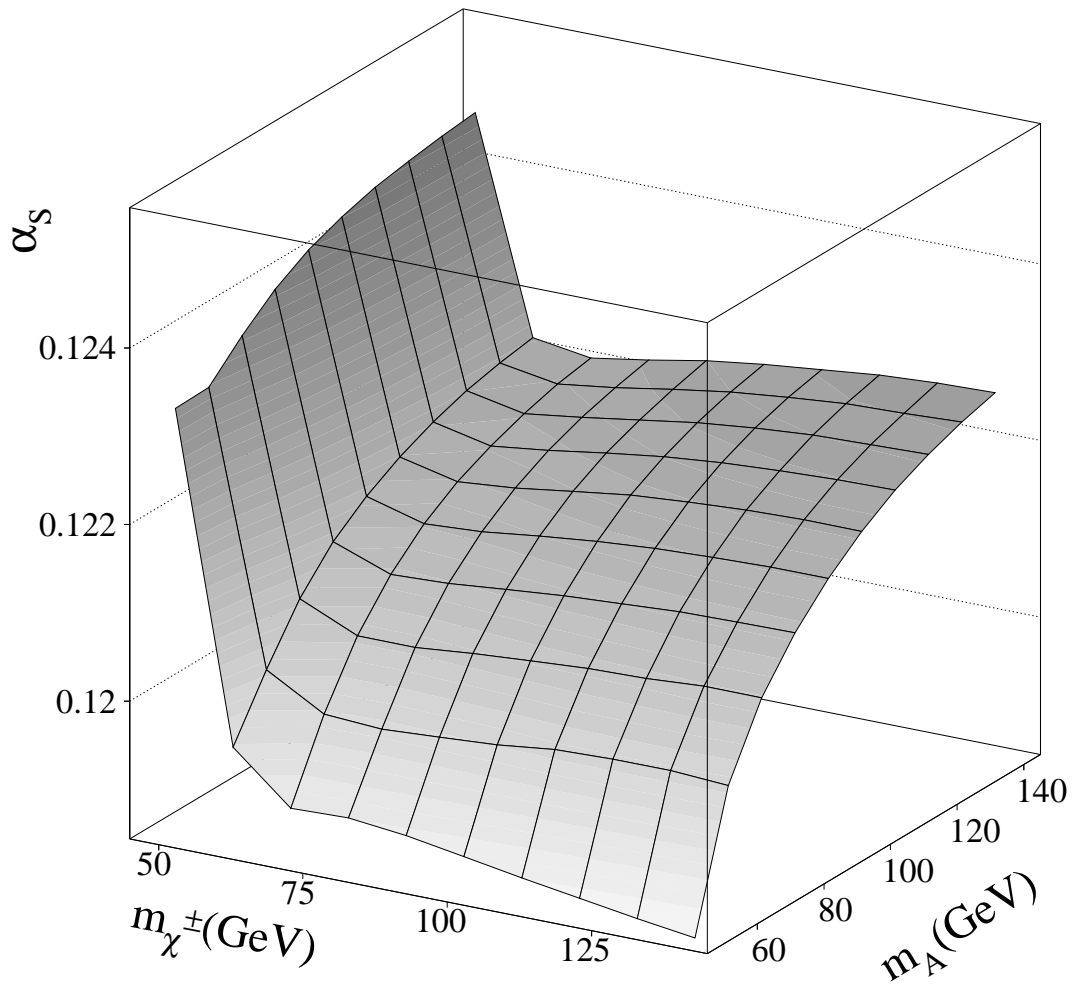


Figure 17: α_s in the pseudoscalar Higgs and light chargino plane for $\tan\beta = 35$. Optimization as in fig. 15.

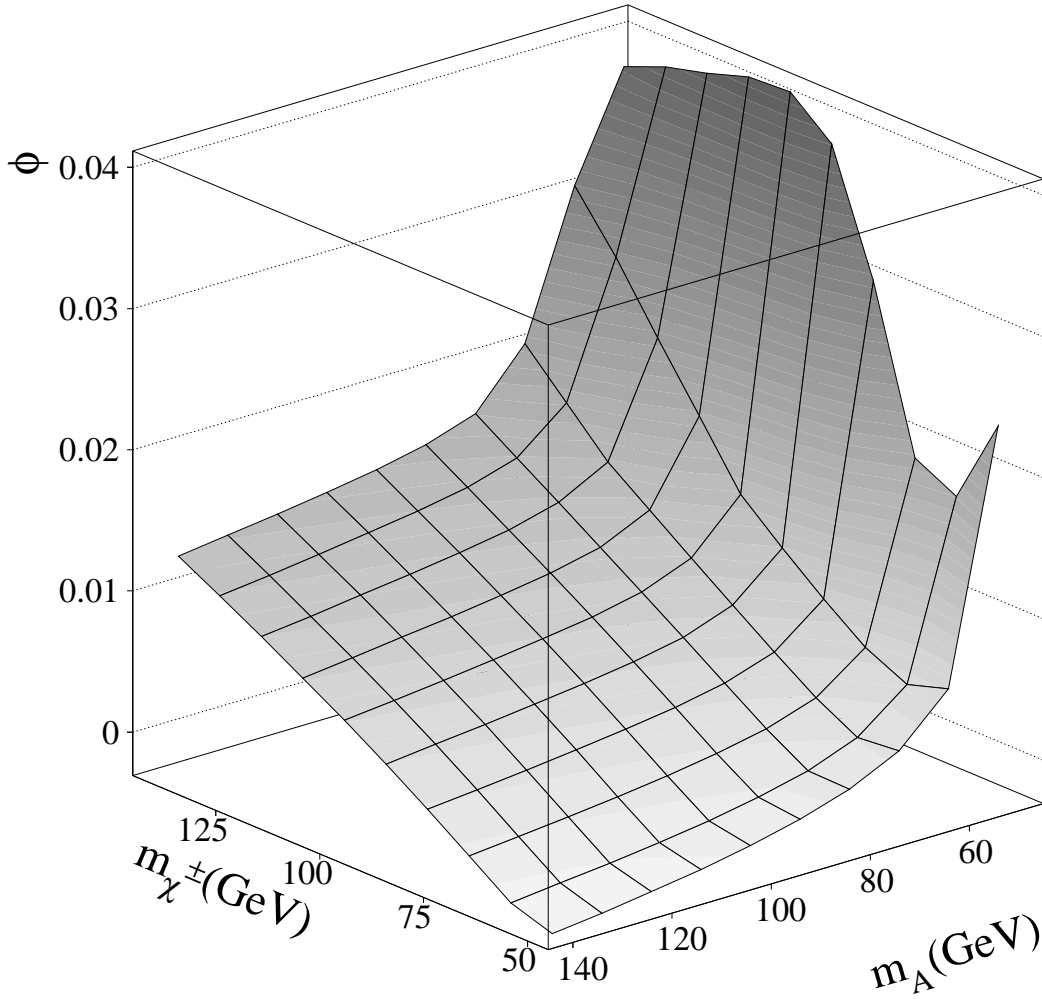


Figure 18: Stop mixing angle ϕ_{mix} in the pseudoscalar Higgs and light chargino plane for $\tan \beta = 35$. Optimization as in fig. 15.

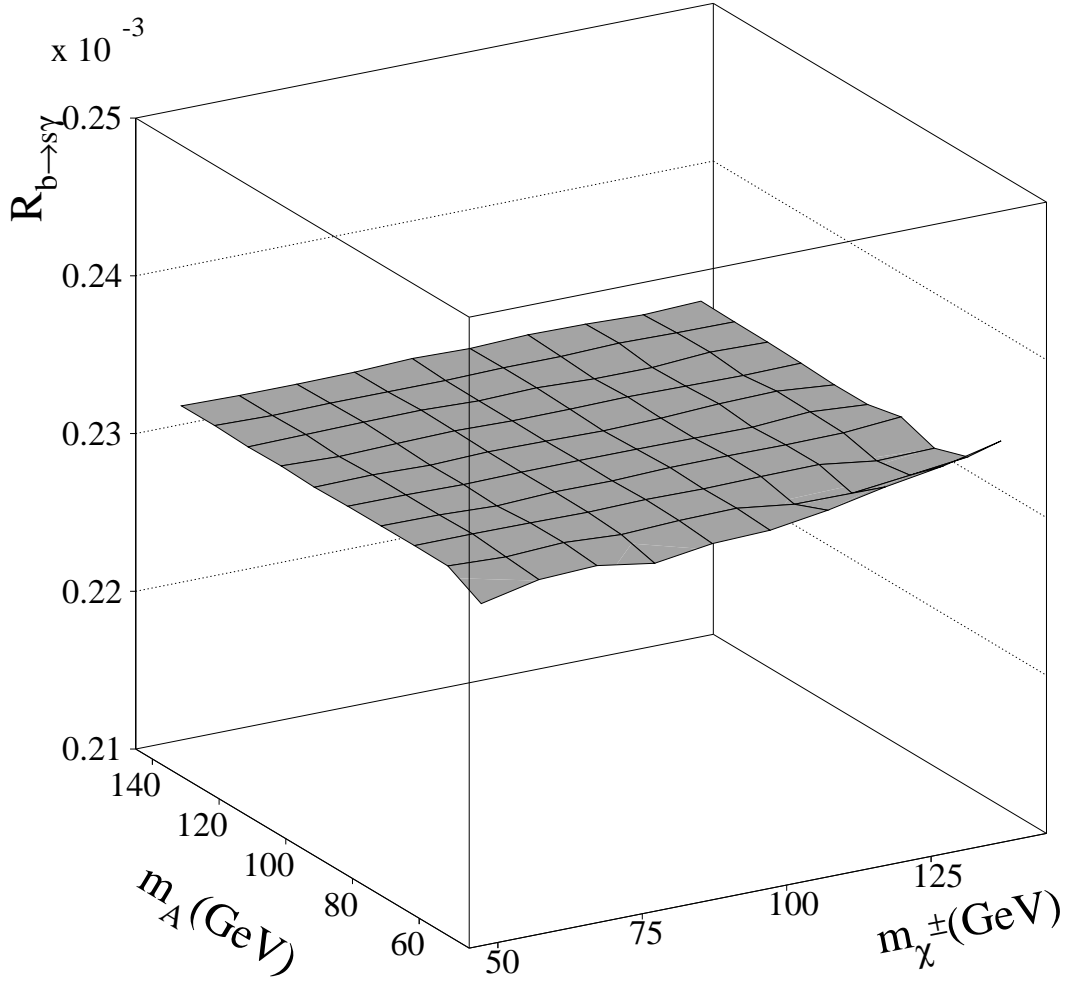


Figure 19: $R_{b \rightarrow s \gamma}$ in the pseudoscalar Higgs and light chargino plane for $\tan \beta = 35$. The prediction is close to the CLEO measurement of $2.32 \pm 0.67 \times 10^{-4}$ within the whole parameter space. Optimization as in fig. 15.

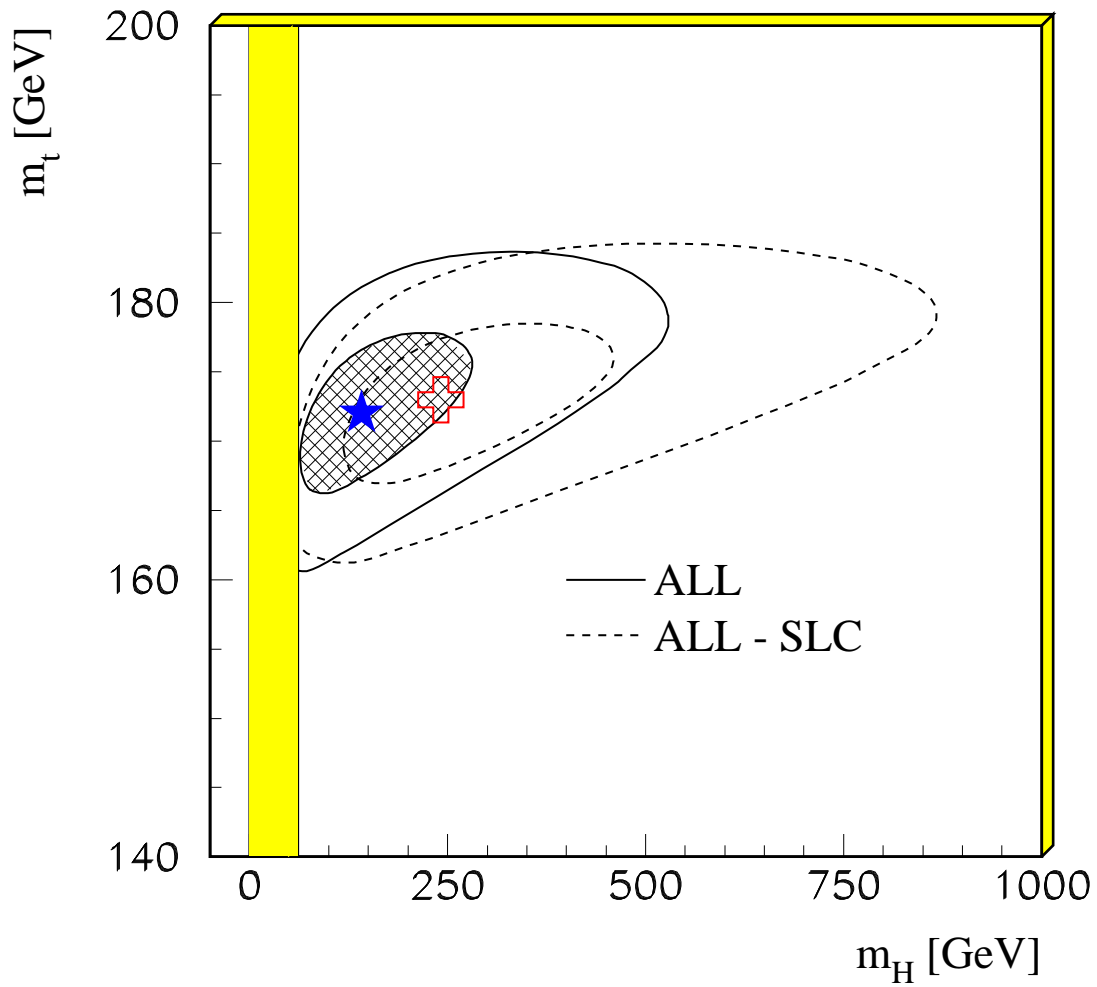


Figure 20: $\Delta\chi^2 = 1$ and $\Delta\chi^2 = 4$ contour lines for all electroweak data including $\sin^2 \theta_{eff}^{lept}$ from SLD (continuous line) and without it (dashed line). The stars indicate the best fits.

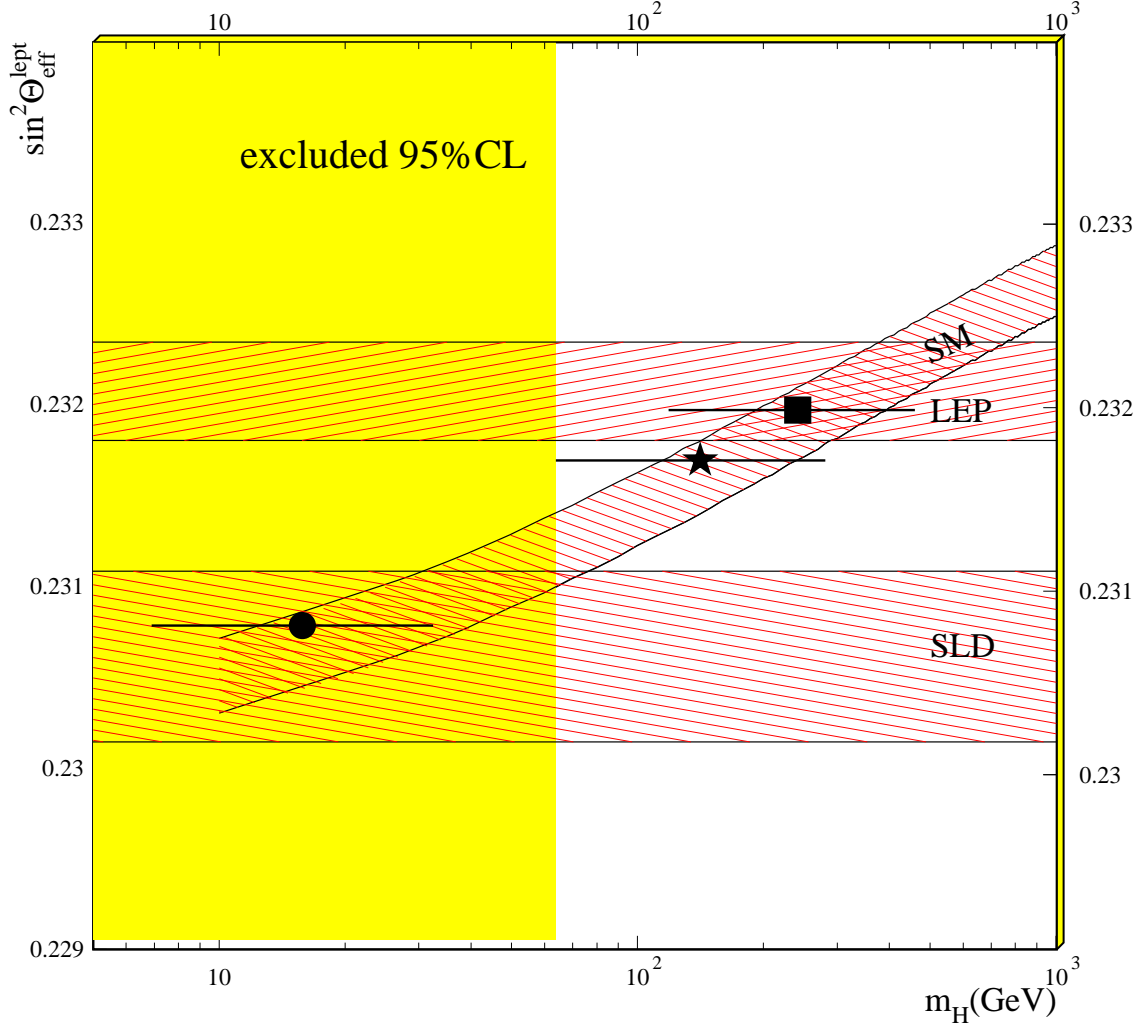


Figure 21: Dependence of the SM $\sin^2 \theta_{eff}^{lept}$ on the Higgs mass. The top mass $m_t = 175 \pm 9$ GeV was varied within its error, as shown by the dashed band labelled SM (upper (lower) boundary $m_t=166(184)$ GeV). The SLD and the LEP measurement of $\sin^2 \theta_{eff}^{lept}$ are also shown as horizontal bands. The star and the square are respectively the results of the combined fit to SLD and LEP data and LEP data without the SLD measurement of $\sin^2 \theta_{eff}^{lept}$, whereas the circle indicates the Higgs mass corresponding to the SLD measurement of $\sin^2 \theta_{eff}^{lept}$. Clearly, the SLD value yields a Higgs mass less than the combined LEP limit of 58.4 GeV (shaded area).

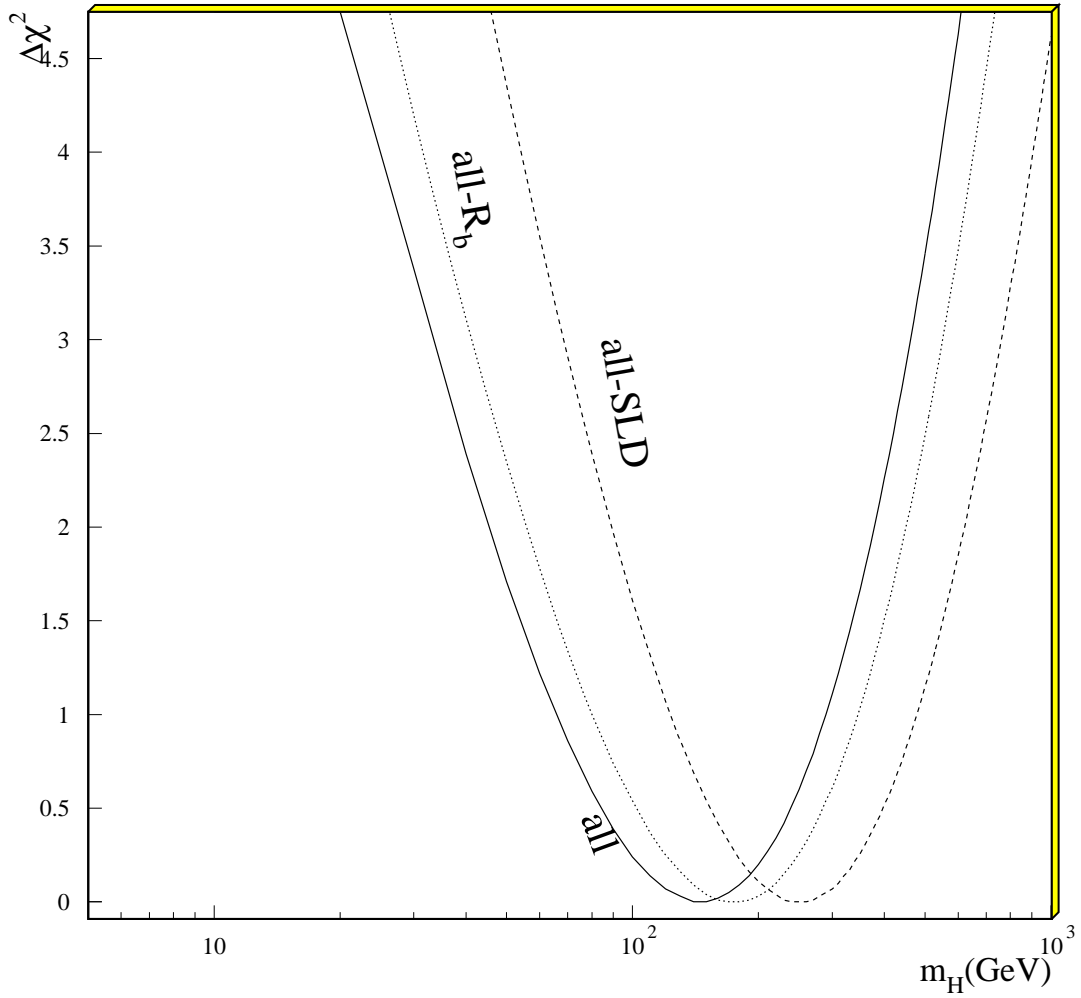


Figure 22: Dependence of the SM $\Delta\chi^2$ on the Higgs mass for a free top mass, taking all data (continuous line), all data without the SLD measurement of $\sin^2\theta_{eff}^{lept}$ (dashed line) and all data without R_b (dotted line).

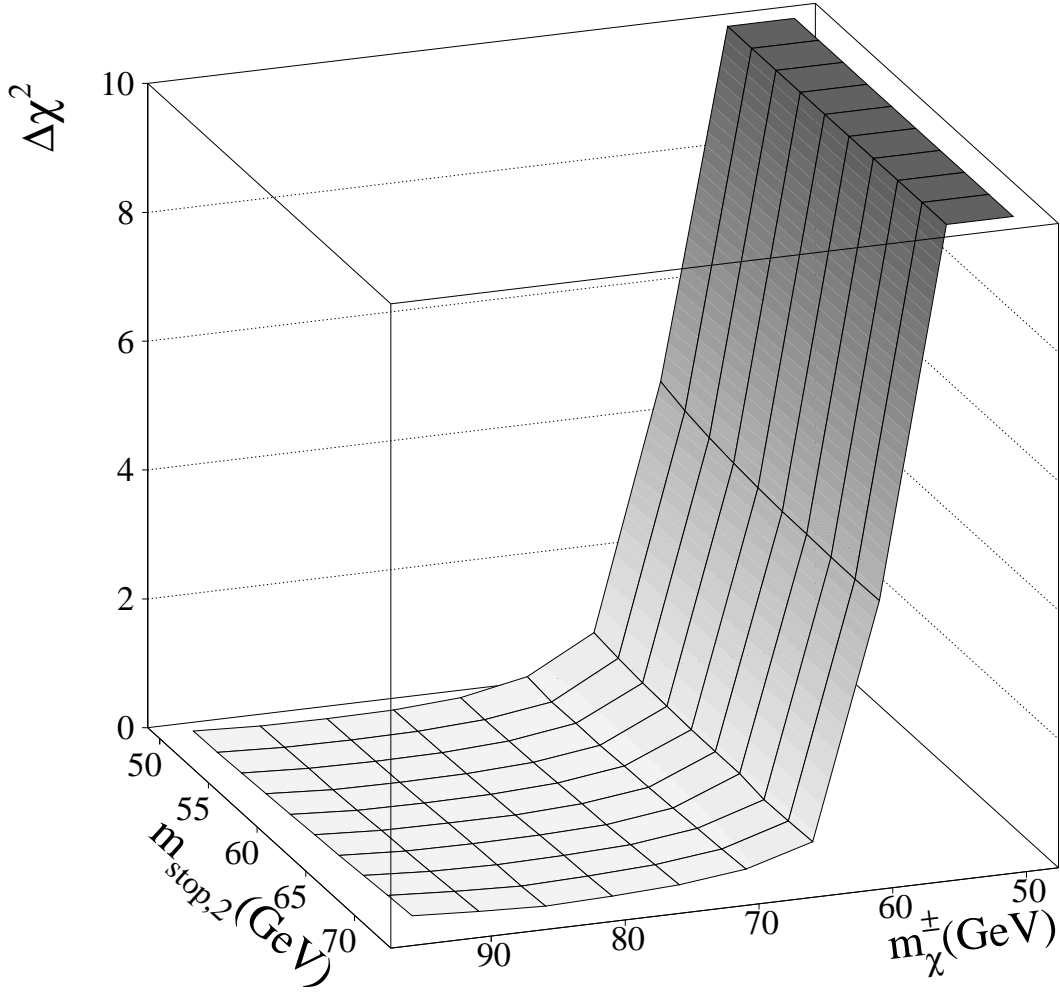


Figure 23: The $\Delta\chi^2$ in the region of the best fit in the light stop and light chargino plane for $\tan\beta = 1.6$. Here the constraint on M_2 was dropped. At each point of the grid an optimization of m_t , M_2 , α_s and the stop mixing angle ϕ_{mix} was performed with $\mu > -40$.

Data / MSSM($\tan\beta = 1.6$)

Data / SM

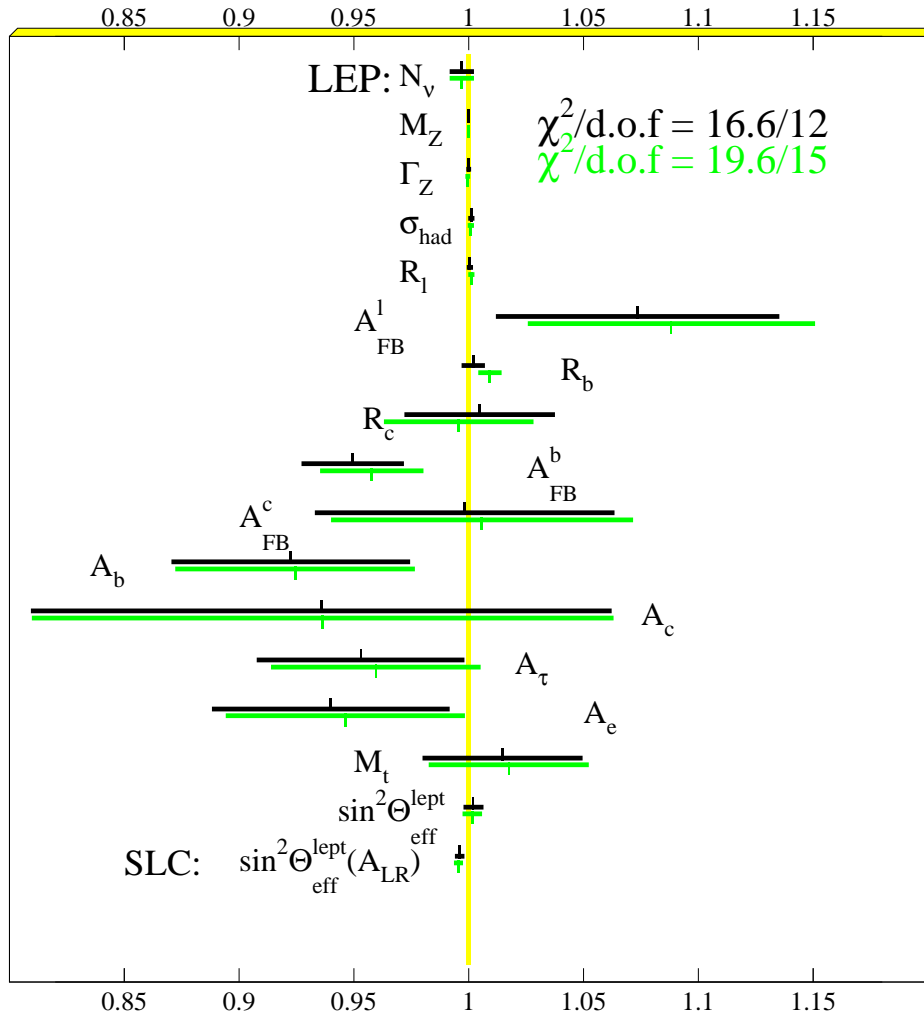


Figure 24: Resulting observables for the fit given in table 3 for $\tan\beta = 1.6$. $m_{\tilde{b}}$ was fixed to 1000 GeV, m_A and the gluino mass were fixed to 1500 GeV. The remaining deviation of R_b from the SM prediction can be fully explained within the MSSM.

Data / MSSM($\tan\beta=35$)
Data / SM

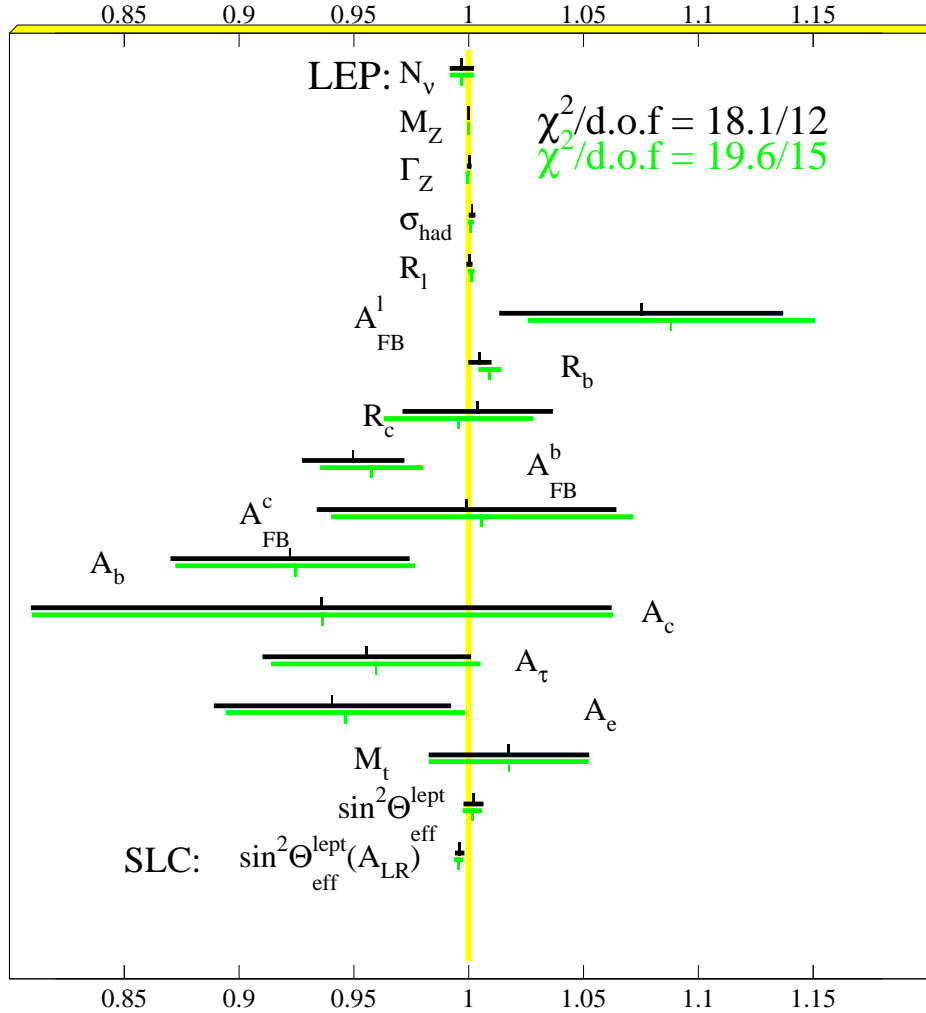


Figure 25: Resulting observables for the fit given in table 3 for $\tan\beta = 35$. $m_{\tilde{b}}$ was fixed to 1000 GeV, M_2 and the gluino mass were fixed to 1500 GeV. It is possible to improve the prediction of R_b with Supersymmetry even for high values of $\tan\beta$, but the result is not as good as for low values.

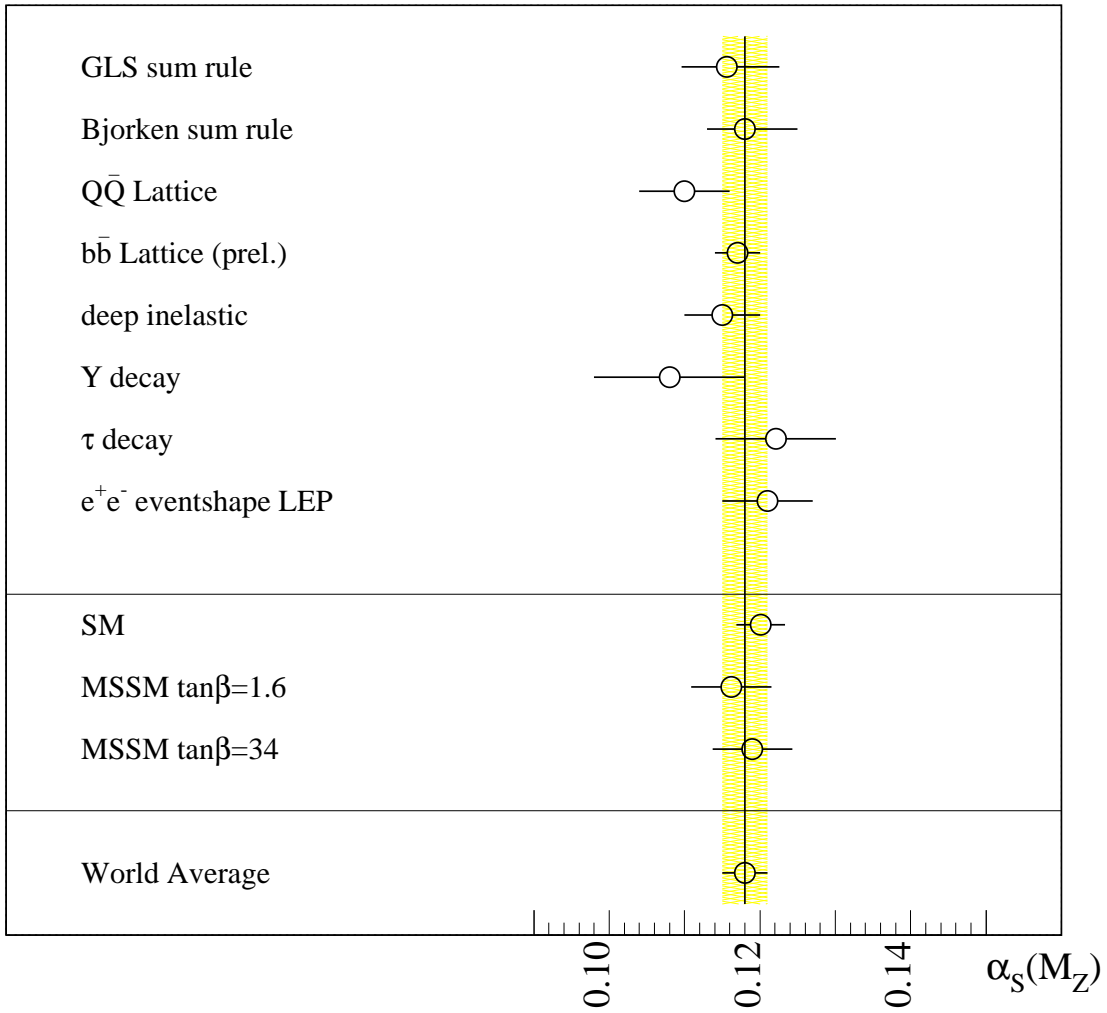


Figure 26: Comparison of different measurements of α_s with our fit results, labeled SM and MSSM. The data has been taken from [11] and [41].

References

- [1] For references see e.g. the review papers:
H.-P. Nilles, *Phys. Rep.* **110** (1984) 1;
H.E. Haber, G.L. Kane, *Phys. Rep.* **117** (1985) 75;
A.B. Lahanas and D.V. Nanopoulos, *Phys. Rep.* **145** (1987) 1; R. Barbieri, *Riv. Nuo. Cim.* **11** (1988) 1;
W. de Boer, *Progr. in Nucl. and Particle Phys.*, **33** (1994) 201. M.F. Sohnius, *Phys. Rep.* **128** (1985) 39;
P. Fayet and S. Ferrara, *Phys. Rep.* **32** (1977) 249.
- [2] F. Abe et al., *CDF Collaboration*, Measurements of the W Boson Mass, *Phys. Rev.* **D52** (1995) 4784;
C. K. Jung, *DØ Collaboration*, W Mass Measurements from DØ and CDF Experiments at the Tevatron, talk given at the 27th ICHEP, Glasgow, Scotland, 20-27 July 1994.
- [3] F. Abe et al., *CDF Collaboration*, *Phys. Rev. Lett.* **74** (1995) 2626, March 1995.
S. Abachi et al., *DØ Collaboration*, *Phys. Rev. Lett.* **74** (1995) 2632, March 1995.;
An updated top mass ($m_t = 175 \pm 6 \text{ GeV}/c^2$) from the combined CDF and D0 data was given by P. Tipton, Plenary talk at 28th Int. Conf. on High Energy Physics, Warsaw, July, 1996;
- [4] A. Blondel, Plenary talk at 28th Int. Conf. on High Energy Physics, Warsaw, July, 1996;
LEP Electroweak Working Group, *Internal Note Warsaw 96* LEPEWWG/96-02, July 1996.
- [5] LEP Electroweak Working Group, *A Combination of Preliminary LEP Electroweak Measurements and Constraints on the Standard Model*, CERN-PPE/95-172; LEP Electroweak Working Group, *Internal Note Moriond 96* LEPEWWG/96-01, March 1996.
- [6] CLEO-Collaboration, R. Ammar et al., *Phys. Rev. Lett.* **74**, (1995) 2885.
- [7] ALEPH Collaboration, *Search for Supersymmetric Particles on e^+e^- Collisions at Centre-of-Mass Energies of 130 and 136 GeV*, CERN-PPE/96-10.
L3 Collaboration, *Search for Supersymmetric Particles at 130 $\leq \sqrt{s} \leq 140$ GeV at LEP*, CERN-PPE/06-29
OPAL Collaboration, *Searches for Supersymmetric Particles and Anomalous Four-Jet Production at $\sqrt{s}=130$ and 136 GeV at LEP*, CERN-PPE/96-096
- [8] OPAL Collaboration, *Topological Search for the Production of Neutralinos and Scalar Particles*, CERN-PPE/96-019;
Search for Chargino and Neutralino Production Using the OPAL Detector at $\sqrt{s} = 130 - 136$ GeV, CERN-PPE/96-020;
DELPHI Collaboration, *Search for the Lightest Chargino at $\sqrt{s} = 130$ and 136 GeV*, CERN-PPE/96-75.
ALEPH Collaboration, *Mass Limit for the Lightest Neutralino*, CERN-PPE/96-083

- [9] D0 Collaboration, *Search for Light Top Squarks in $p\bar{p}$ Collisions at 1.8 TeV*, *Phys. Rev. Letters* **76**, 2222 (1996) , FERMILAB-PUB-95/380-E;
DELPHI Collaboration, *Search for neutralinos, scalar leptons and scalar quarks in e^+e^- interactions at $\sqrt{s}=130$ GeV and 136 GeV*, CERN-PPE/96-110
OPAL Collaboration, *Search for Scalar Top and Scalar Bottom Quarks using the OPAL Detector at LEP*, CERN-PPE/96-133
- [10] ALEPH Collaboration, *Mass Limit for the Standard Model Higgs Boson with the full LEP I ALEPH Data Sample*, CERN PPE/96-079.
- [11] R.M. Barnett et al., *Phys. Rev.* **D54** (1996) 1.
- [12] D. Bardin et al., *ZFITTER, An Analytical Program for Fermion Pair Production in e^+e^- Annihilation*, CERN-TH.6443/92.
- [13] A. Dabelstein, *Z. Phys.* **C67** (1995) 495; *Nucl. Phys.* **B456** (1995) 25; A. Dabelstein, W. Hollik, W. Möhle, in preparation.
- [14] F. James, *MINUIT Reference Manual*, Version 94.1, Computing and Networks Division CERN Geneva, Switzerland.
- [15] *Proceedings of the Workshop Physics at LEP2* , Editors G. Altarelli, T. Sjöstrand, F. Zwirner, Vol.1 and Vol.2, CERN 96-01.
- [16] M. Boulware, D. Finnell, *Radiative Corrections to $BR(Z \rightarrow b\bar{b})$ in the Minimal Supersymmetric Standard Model*, *Phys. Rev.* **D44**(1991) 2054.
- [17] P. H. Chankowski, S. Pokorski, *Chargino Mass and R_b Anomaly* , *Nucl. Phys.***B475** (1996) 3-26, hep-ph 9603310.
- [18] J. Ellis, J. L. Lopez, D. V. Nanopoulos, hep-ph/9512288.
- [19] D. Garcia, J. Sola, *The Quantum Correlation $R_b - R_c$ in the MSSM: More Hints of Supersymmetry?* , hep-ph/9502317, *Phys. Lett.* **B354** (1995) 335.
- [20] G.L. Kane, R.G. Stuart, J.D. Wells, *A Global Fit of LEP/SLC Data with Light Superpartners*, *Phys. Lett.* **B354**(1995) 350, UM-TH-94-16, hep-ph/9505207.
- [21] J.D. Wells, C. Kolda, G.L. Kane, *Implications of $\Gamma(Z \rightarrow b\bar{b})$ for Supersymmetry Searches and Model-Building* , *Phys. Lett.* **B338**(1993) 219, UM-TH-94-23, hep-ph/9408228.
- [22] D. Garcia, R. Jimenez, J. Sola, *Supersymmetric Electroweak Renormalization of the Z Width in the MSSM.**Phys. Lett.* **B347** (1995) 309; *Phys. Lett.* **B347** (1995) 321.
- [23] D. Garcia, J. Sola, *Matching the low-Energy and the high-Energy Determinations of $\alpha_s(M(Z))$ in the MSSM*,*Phys. Lett.* **B357**(1995) 349.
- [24] C. Greub, T. Hurth, *Towards a next-to-leading logarithmic result in $B \rightarrow X_s\gamma$* , SLAC-PUB-7267, ITP-SB-96-46, hep-ph/9608449;
M. Misiak, talk given at 28th Int. Conf. on High Energy Physics, Warsaw, July, 1996.

- [25] A. Sirlin, *Phys. Rev. D* **22** (1980) 971.
W. J. Marciano and A. Sirlin, *Phys. Rev. D* **22** (1980) 2695.
- [26] D. Garcia and J. Solà, *Mod. Phys. Lett. A* **9** (1994) 211.
P.H. Chankowski, A. Dabelstein, W. Hollik, W. Möhle, S. Pokorski and J. Rosiek, *Nucl. Phys. B* **417** (1994) 101.
- [27] For a recent review see: *Precision Calculations for the Z Resonance*, Yellow report CERN 95-03, eds. D. Bardin, W. Hollik and G. Passarino, and references therein.
- [28] L. Avdeev, J. Fleischer, S. Mikhailov and O. V. Tarasov, *Phys. Lett. B* **336** (1994) 560.
J. Fleischer, O. V. Tarasov and F. Jegerlehner, *Phys. Lett. B* **319** (1993) 249;
R. Barbieri, M. Beccaria, P. Ciafaloni, G. Curci, A. Vicere, *Phys. Lett. B* **288** (1992) 95; *ibid.* **B409** (1993) 105;
K.G. Chetyrkin, J.H. Kühn, M. Steinhauser, *Phys. Lett. B* **351** (1995) 331;
J. Fleischer, F. Jegerlehner, P. Raczka, O.V. Tarasov, *Phys. Lett. B* **293** (1992) 437;
G. Buchalla, A.J. Buras, *Nucl. Phys. B* **398** (1993) 285.
- [29] K. G. Chetyrkin, J. H. Kühn and A. Kwiatkowski, *Phys. Lett. B* **282** (1992) 221;
K. G. Chetyrkin and A. Kwiatkowski, *Phys. Lett. B* **305** (1993) 285;
K. G. Chetyrkin, A. Kwiatkowski and M. Steinhauser, *Mod. Phys. Lett. A* **29** (1993) 2785;
A. Kwiatkowski, M. Steinhauser, *Phys. Lett. B* **344** (1995) 359;
K. G. Chetyrkin, J. H. Kühn and A. Kwiatkowski, in: *Precision Calculations for the Z Resonance*, CERN 95-03, eds. D. Bardin, W. Hollik, G. Passarino
S. Peris, A. Santamaria, CERN-TH-95-21 (1995).
- [30] M. Böhm, W. Hollik and H. Spiesberger, *Fortschr. Phys.* **34** (1986) 687.
W. Hollik, *Fortschr. Phys.* **38** (1990) 165.
- [31] A. Denner, R. Guth, W. Hollik, J.H. Kühn, *Z. Phys. C* **51** (1991) 695.
- [32] H. P. Nilles, *Phys. Rep.* **110** (1984) 1.
H. E. Haber and G. Kane, *Phys. Rep.* **117** (1985) 75.
J. F. Gunion and H. E. Haber, *Nucl. Phys. B* **272** (1986) 1; *Nucl. Phys. B* **402** (1993) 567. J. F. Gunion, H. E. Haber, G. Kane and S. Dawson: *The Higgs Hunter's Guide*, Addison-Wesley 1990.
- [33] J. Ellis, G. Ridolfi and F. Zwirner, *Phys. Lett. B* **257** (1991) 83.
- [34] R. Barbieri, G. Gamberini, G. Giudice, G. Ridolfi, *Nucl. Phys. B* **296** (1988) 75-90.
- [35] R. Barbieri and G. Giudice, *Phys. Lett. B* **309** (1993) 86;
R. Garisto and J.N. Ng, *Phys. Lett. B* **315** (1993) 372;
S. Bertolini, F. Borzumati, A. Masiero, and G. Ridolfi, *Nucl. Phys. B* **353** (1991) 591
and references therein;
N. Oshimo, *Nucl. Phys. B* **404** (1993) 20;
S. Bertolini, F. Vissani, *Z. Phys. C* **67** (1995) 513, 1995.

- [36] S. Eidelman and F. Jegerlehner, *Z. Phys.* **C67** (1995) 585;
H. Burkhardt and B. Pietrzyk, *Phys. Lett.* **B356**(1995) 398.
- [37] R. Ehret, *Die Bestimmung der Kopplungskonstanten α_s am LEP-Speicherring und Tests von großen Vereinigungstheorien* , Ph.D. Thesis, Univ. Karlsruhe, IEKP-KA/95-13.
- [38] W. de Boer et al., *Combined Fit of Low Energy Constraints to Minimal Supersymmetry and Discovery Potential at LEP II*, hep-ph/9603350; W. de Boer et al., *Predictions of SUSY masses in the minimal supersymmetric grand unified theory*, *Z. Phys.* **C67**, (1995) 647-664.
- [39] W. de Boer et al., *MSSM predictions of the Neutral Higgs Boson Masses And LEP- II Production Cross- Sections* , hep-ph/9603346 and references therein.
- [40] J. Ellis, G.L. Fogli, E. Lisi, *Indications from Precision Electroweak Physics Confront Theoretical Bounds on the Mass of the Higgs Boson*, CERN-TH/96-216, hep-ph/9608329.
- [41] M. Schmelling, Plenary talk at 28th Int. Conf. on High Energy Physics, Warsaw, July, 1996.